Aus der Klinik und Poliklinik für Nuklearmedizin der
Ludwig-Maximilians-Universität München
Direktor: Prof. Dr. med. P. Bartenstein

Untersuchungen der Amyloid-Pathologie an einem transgenen Alzheimer-Mausmodell mittels Positronen-Emissions-Tomographie

Dissertation
zum Erwerb des Doktorgrades der Medizin
an der Medizinischen Fakultät der
Ludwig-Maximilians-Universität zu München

vorgelegt von

Matthias Brendel
aus
Marktoberdorf

Jahr
2015

Mit Genehmigung der Medizinischen Fakultät
der Universität München

Berichterstatter:	PD Dr. med. Axel Rominger
Mitberichterstatter:	Prof. Dr. med. Oliver Pogarell Prof. Dr. med. Jochen Herms PD Dr. med. Johannes Levin
Dekan:	Prof. Dr. med. Dr. h.c. M. Reiser, FACR, FRCR
Tag der mündlichen Prüfung:	12.03.2015

Die vorliegende kumulative Dissertation umfasst zwei bereits publizierte Manuskripte:

Rominger, A.*, **Brendel, M**.*, Burgold, S., Keppler, K., Baumann, K., Xiong, G., Mille, E., Gildehaus, F.J., Carlsen, J., Schlichtiger, J., Niedermoser, S., Wangler, B., Cumming, P., Steiner, H., Herms, J., Haass, C., Bartenstein, P., 2013. **Longitudinal assessment of cerebral beta-amyloid deposition in mice overexpressing Swedish mutant beta-amyloid precursor protein using 18F-florbetaben PET.** J Nucl Med. 2013 54(7):1127-34.

* Geteilte Erstautorenschaft

Brendel, M., Delker, A., Rotzer, C., Boning, G., Carlsen, J., Cyran, C., Mille, E., Gildehaus, F.J., Cumming, P., Baumann, K., Steiner, H., Haass, C., Herms, J., Bartenstein, P., Rominger, A., 2013. **Impact of partial volume effect correction on cerebral beta-amyloid imaging in APP-Swe mice using [^{18}F]-florbetaben PET**. Neuroimage. 2014 84:843-53.

Kumulative Dissertation gemäß § 4a der Promotionsordnung

Inhalt

1. Einführung

Die Alzheimer Erkrankung stellt trotz intensiver Bemühungen weltweiter Forschung in Wissenschaft und Industrie weiterhin ein gravierendes sozioökonomisches Problem dar, welches vor allem in den Industrienationen zur Geltung kommen wird (Ziegler-Graham, Brookmeyer et al. 2008). Dies wird zum einen begründet durch den fortschreitenden demographischen Wandel, welcher in den kommenden Dekaden zu einem massiven Anstieg des Bevölkerungsanteils von 65 Jahren und darüber führen wird und zum anderen aufgrund fehlender potenter Interventionsmöglichkeiten (Schneider 2013). Aktuelle Leitlinien der Deutschen Gesellschaft für Neurologie empfehlen je nach Zeitpunkt der klinischen Diagnose, den Einsatz von Acetylcholinesterasehemmern (frühe Stadien) und NMDA Antagonisten (fortgeschrittene Stadien). Hiermit lässt sich jedoch nur eine geringfügige Verzögerung der Progression der Erkrankung erreichen (Schneider 2013).

1.1 Amyloid-Pathologie

ß-Amyloid stellt ein Protein verschiedener Isoformen (hauptsächlich Aß38, Aß40 und Aß42) dar, welche durch Enzyme der Gamma Sekretase Klasse am Amyloid Precursor Protein (APP) abgespalten werden. Akkumulierung von ß-Amyloid führt zu plaqueförmigen Ablagerungen im humanen Gehirn weit vor Auftreten der ersten Symptome der Alzheimer Erkrankung. Neueste Ergebnisse der ß-Amyloid Bildgebung an Probanden der australischen Bevölkerung deuten sogar darauf hin, dass der Verlauf von ersten detektierbaren Plaques bis hin zur manifesten Alzheimer Demenz zwei bis drei Dekaden in Anspruch nimmt (Villemagne, Burnham et al. 2013). Auch in ungefähr 50% der Fälle einer Lewy-Body Demenz aggregiert das Protein

vermehrt, wobei dennoch gezeigt werden konnte, dass ß-Amyloid in neuronalen Signalwegen wie dem Notch-Signalweg von essentieller Bedeutung ist (Wolfe 2012). Die zweite Frühmanifestation im Gehirn von Alzheimer Patienten stellt das Protein Tau dar, welches auch im Zuge einer Cortikobasalen Degeneration, Fronto-Temporaler Demenz und der Progressiven Supranukleären Blickparese zu beobachten ist. ß-Amyloid und Tau Aggregation wiederum führen nach neuesten Erkenntnissen zu erhöhter Neuroinflammation, welche letztlich die Endstrecke des neuronalen Zelluntergangs darstellt (Palop and Mucke 2010). Ein umfassendes Verständnis der Pathogenese verbleibt jedoch vorerst Gegenstand intensiver aktiver Forschung.

1.2 Amyloidogenese als therapeutisches Target

In der aktuellen pharmakologischen Forschung stellt unter anderem die Gamma Sekretase einen möglichen Angriffspunkt zur Unterbrechung der Amyloidogenese dar, wobei die ersten Überlegungen dazu tendierten, mit Inhibitoren des Enzyms (GSI) die Kaskade der Proteinabspaltung zu blockieren (Schenk, Basi et al. 2012). Hierbei wurde festgestellt, dass durch eine Inhibition ein Ungleichgewicht der verschiedenen Isoformen entsteht, welches auch den physiologischen Notch-Signalweg unterbricht, der neben seiner Funktion im embryonalen Zellwachstum auch für Erneuerung und Aufrechterhaltung des adulten Gewebes eine große Rolle spielt. Zum anderen ergaben sich in ersten klinischen Studien ein ungünstiges Wirkungs- und Nebenwirkungsprofil. Bei 14 wöchiger Verabreichung des unselektiven GSI Semigacestat an Patienten mit milder bis mäßiger Alzheimer Erkrankung ergab sich keine Verbesserung der kognitiven

Fähigkeiten im Vergleich zu einem Placebo. Zudem traten in der GSI Gruppe mehr Nebenwirkungen, wie gastrointestinale Beschwerden und Hautausschlag auf (Fleisher, Raman et al. 2008). Auch bei dem GSI Avagacestat, für welchen eine höhere Selektivität für die β-Amyloid Synthese als für den Notch Signalweg postuliert wurde, kam es zu ähnlichen dosisabhängigen Nebenwirkungen (Coric, van Dyck et al. 2012). Bei einer Dosis von 100 bzw. 125 mg/Tag wurde sogar eine Verschlechterung der kognitiven Fähigkeiten beobachtet. Daraufhin veränderte sich die pharmakologische Strategie, unter anderem in Richtung einer Gamma Sekretase Modulation (GSM), welche zu einer Reduktion des ß-Amyloid42 bei gleichbleibenden anderweitigen Isoformen führen sollte. In klinischen Placebo-kontrollierten Studien, konnte bei Tarenflurbil, welches ein Derivat eines nicht-steroidalen Antiphlogistikums (NSAP) darstellt, jedoch auch keine Besserung der kognitiven Fähigkeiten nachgewiesen werden (Green, Schneider et al. 2009). Ein weiterer GSM, E2212 (nicht-NSAP), zeigte bei Verabreichung an gesunden Probanden im Vergleich zum Placebo dosisunabhängige Nebenwirkungen wie Diarrhö, Kopfschmerz, Schwindel und orthostatische Hypotonie. Es konnte keine Aussage bezüglich der Wirksamkeit gemacht werden (Yu, Logovinsky et al. 2013).

1.3 Amyloid-Bildgebung

Die molekulare Bildgebung mittels der Positronen-Emissions-Tomographie (PET) stellt im Bereich der Diagnostik und der Erforschung der Alzheimer Erkrankung einen schnell wachsenden Sektor dar. Radioaktiv markierte Trägerstoffe (Radiotracer) ermöglichen seit Mitte des vergangenen Jahrzehntes die Detektion von zerebralen ß-Amyloid Ablagerungen *in vivo*

(Klunk, Engler et al. 2004), welche zusammen mit dem hyperphosphorylierten Tau-Protein wahrscheinlich einen entscheidenden Einfluss in der Pathogenese der Erkrankung darstellen (LaFerla 2010). Begründet durch die mit 20,3 Minuten extrem kurze Halbwertszeit von [^{11}C] bestand mit dem ersten β-Amyloid-Tracer [^{11}C]-Pittsburgh Compound B (PiB) eine Beschränkung auf Zentren mit unmittelbarem Zugang zu einem Zyklotron. Eine breitere Verfügbarkeit von ß-Amyloid Radiotracern konnte durch die in den vergangenen Jahren etablierten Fluor-markierten Substanzen [^{18}F]-Florbetaben (Barthel and Sabri 2011), [^{18}F]-Florbetapir (Clark, Schneider et al. 2011) und [^{18}F]-Flutemetamol (Vandenberghe, Van Laere et al. 2010) (Halbwertszeit 109,8 min) erreicht werden. Somit existiert für den humanen Bereich aktuell eine sensitive und verlässliche Frühdiagnostik bei Fehlen suffizienter Therapiemöglichkeiten, was eine nicht zu unterschätzende ethische Problematik aufwirft (Visser, Wolf et al. 2012). Dennoch trägt die Verfügbarkeit der *in vivo* Diagnostik entscheidend dazu bei, neue Erkenntnisse in der longitudinalen Entwicklung der Alzheimer Erkrankung zu erlangen und insbesondere Patienten zu selektieren, welche anti-Amyloid Therapiestudien zugeführt werden können.

1.4 Kleintier Modelle der Alzheimer Demenz

Präklinisch existieren im Alzheimer Sektor eine Vielzahl verschiedener genetischer Mutationen, (Teipel, Buchert et al. 2011) welche durch Klonierung oder Insertion in Maus- oder Rattenstämme eingebracht werden können. Diese wurden durch familiär existente Häufungen im Humanbereich identifiziert und bestehen primär aus Veränderungen in den APP-, Presenilin1/2- oder Apolipoprotein-E Genen. Sowohl humane als auch

murine Genkonstrukte können hierbei verwendet werden. Kombinationen dieser Genmutationen ermöglichen mehrfach transgene Stämme (Oakley, Cole et al. 2006), welche durch schnelleres Einsetzen der Pathologie und durch beschleunigtes Fortschreiten der Plaquemanifestation gekennzeichnet sind. Eine hohe Variabilität in der Ausprägung der Plaquemanifestation ist nahezu allen diesen Modellorganismen zu Eigen. Einbezogen werden muss ebenfalls die Nähe des Modelles zur humanen Pathologie, welche bei einer Beschränkung auf APP Mutationen am ehesten gegeben ist, jedoch zum Nachteil hat, dass durch die späte Manifestation und die langsame Progression ein längerer Beobachtungszeitraum in Studienplanungen berücksichtigt werden muss. APP-Swe Mäuse mit C57Bl/6 Hintergrund (Richards, Higgins et al. 2003) stellen ein solches Modell dar und weisen eine, auf eine doppelte APP Mutation (sogenannte Schwedische Mutation) beschränkte Transgenität auf. Die Plaquebildung setzt in APP-Swe Mäusen im Alter von ungefähr 9 Monaten ein, bei einer primären Manifestation im Cortex.

1.5 Kleintier PET

Durch die Weiterentwicklung der PET Technologie ist eine Anwendung im Kleintierbereich mit speziell dafür konfigurierten Scannern möglich (Visser, Disselhorst et al. 2009), wobei hier die räumliche Auflösung in Relation zur Größe der Zielstrukturen den entscheidenden limitierenden Faktor darstellt. Die PET hat, im Gegensatz zu histologischen Untersuchungen, den entscheidenden Vorteil, auch im Mausmodell *in vivo* Untersuchungen durchführen zu können. Dadurch können sowohl Analysen zum Startzeitpunkt einer Studie erhoben werden, als auch der longitudinale

Verlauf in einem einzelnen Individuum betrachtet werden. Dies bringt gerade in hochvariablen Modellorganismen einen entscheidenden Vorteil, da nicht nur der Endpunkt, wie in histologischen Untersuchungen, sondern auch die individuelle Kinetik beurteilt werden kann. Verbesserte Rekonstruktionsalgorithmen (Cheng, Shoghi et al. 2012) und der Einsatz von aus Plexiglas konfigurierten Mehrfach-Maushalterungen (Rominger, Mille et al. 2010) haben das Verfahren in Sensitivität und Ökonomie weiterentwickelt, so dass bis zu acht Mäuse zeitgleich in einer räumlichen Auflösung von unter 1.5 mm gemessen werden können.

1.6 Kleintier PET Studien zur Detektion von Amyloid-Ablagerungen

Die bis zum Zeitpunkt unserer Arbeit durchgeführten ß-Amyloid PET Kleintierstudien lieferten weltweit diskrepante Ergebnisse. So zeigten sich in den initialen Versuchen entweder nur geringe Unterschiede zwischen transgenen Tieren und Kontrollen, unter Verwendung von [^{11}C]-PiB und dem Tg2576 Mausmodell (Toyama, Ye et al. 2005) oder sogar ein niedrigeres PET Signal in Tg2576 Tieren gegenüber Kontrollen, die mittels [^{18}F]-FDDNP gemessen wurden (Kuntner, Kesner et al. 2009). Maeda und Koautoren waren die Ersten, die ein ansteigendes PET Signal in einem longitudinalen Versuchsaufbau mittels [^{11}C]-PiB und 17-27 Monate alten Tieren des APP23 Mausmodelles zeigen konnten (Maeda, Ji et al. 2007). Auch in ARTE10 Mäusen konnte unter Verwendung von [^{11}C]-PiB in einer multimodalen Analyse ein höheres PET Signal in alten transgenen Tieren im Gegensatz zu jungen transgenen Tieren und nicht-transgenen Kontrollen gemessen werden, welches sich in Übereinstimmung mit der Histologie zeigte (Manook, Yousefi et al. 2012). Dahingegen zeigte sich in APP/PS1-21 Mäusen zwar

eine Erhöhung des [^{18}F]-Florbetapir PET Signales schon im Alter von 5 Monaten, jedoch kein weiterer Anstieg bei 8 und 12 Monaten im Gegensatz zur Histologie, in welcher das Modell durch eine weitere Zunahme der cortikalen Plaqueload gekennzeichnet ist (Poisnel, Dhilly et al. 2012).

1.7 Partialvolumeneffekte in der Kleintier PET

Eine Schwierigkeit in der Bildgebung mittels PET - vor allem im Dimensionsbereich von Kleintieren - stellen Partialvolumeneffekte dar. Diese entstehen durch die relativ geringe räumliche Auflösung der zur Kleintier-Bildgebung geeigneten Geräte im Verhältnis zu den Zielstrukturen (z.B. 1 mm Dicke des Frontalgehirnes einer Maus) und äußern sich in einer Verflachung der maximal zu erwartenden Signalhöhe bei Streuung in die Umgebung. So werden beispielsweise bei einer Zunahme der Pathologie die zu erwartenden Signalerhöhungen falsch zu niedrig berechnet. Goldstandard Untersuchungen mittels Autoradiographie (Analyse der Gehirnschnitte im µm Bereich mit entsprechend hoher Ortsauflösung) haben dies bewiesen (Toyama, Ichise et al. 2004). Dennoch gibt es im Kleintierbereich noch sehr wenige Studien, welche sich mit der Korrektur dieser Partialvolumeneffekte auseinander setzen (Nandoe Tewarie, Yu et al. 2010; Lehnert, Gregoire et al. 2012).

2. Inhalte der Promotionsarbeit

2.1 Longitudinale Evaluierung eines Mausmodelles mittels Amyloid-PET

Im Rahmen meiner Promotion wurde zunächst die ß-Amyloid Kleintier PET mittels [^{18}F]-Florbetaben in einem longitudinalen Versuchsaufbau etabliert und validiert. Hierbei wurden oben beschriebene transgene APP-Swe Mäuse ab einem Alter von 10/13 Monaten über 3/7 Monate verfolgt. Neben der Planung und Durchführung der Experimente galt das Hauptaugenmerk hierbei der Entwicklung eines robusten und verlässlichen Algorithmus für die Auswertung der erhobenen Bilddaten. Initial wurde hierfür das Aufnahmemuster von [^{18}F]-Florbetaben im Gehirn der Maus mittels eines Dualscans mit [^{18}F]-Fluordesoxyglucose abgeglichen. Auf Grundlage dieser Information wurden anschließend C57Bl/6 Tiere gescannt und die Bilddaten durch eine rigide manuelle Co-Registrierung auf ein standardisiertes anatomische Template (kranialer Magnetresonanztomografie-Atlas) des Mäusegehirnes fusioniert. Durch die Summation dieser räumlich normalisierten Daten entstand daraufhin ein [^{18}F]-Florbetaben Template, welches für die exakte Co-Registrierung der Folgedaten verwendet werden konnte. Mittels Festlegung drei-dimensionaler Zielvolumina in der Anatomie des MRT-Atlas (**Abb. 1**) wurden die PET Daten der longitudinalen Studie anschließend sowohl dynamisch (0-90 min) als auch in verschiedenen statischen Zeitfenstern (20-50, 30-60, 40-70 min) ausgewertet, wobei das Kleinhirn als Referenzgewebe für die Normalisierung der variablen Traceraufnahme verwendet wurde. Der entsprechende Zielparameter besteht hier im Verhältnis des standardisierten Aufnahmewertes im Cortex/Hippocampus gegenüber dem Kleinhirn ($SUVR_{CTX/CBL}$; $SUVR_{HIP/CBL}$).

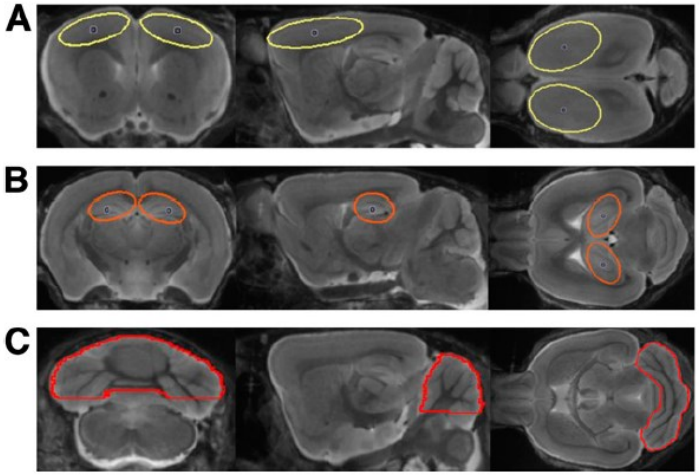

Abbildung 1: Definitionen von cortikalen (gelb) (**A**), hippocampalen (orange) (**B**), und cerebellären (rot) (**C**) Zielvolumina im MRT-Atlas des Mausgehirnes in coronalen, sagittalen und axialen Schnitten.

Wir konnten zeigen, dass ein statisches 30-60 Minuten Zeitfenster ein stabiles Signal liefert und sich äquivalent zu einer dynamischen 90 Minuten Messung verhält (**Abb. 2**).

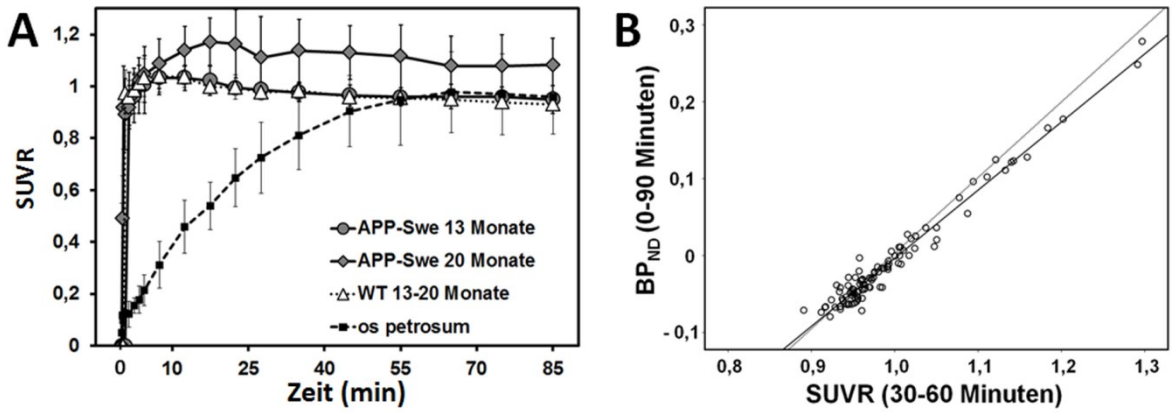

Abbildung 2: (**A**) Zeitaktivitätskurven des cortikalen Signales (SUVR ± Stabw.) in der dynamischen 90 Minuten Messung für APP-Swe Tiere im Alter von 13 Monaten (N = 10; grau, Kreis) und 20 Monaten (N = 5; grau, Raute), sowie für C57Bl/6 (WT) Tiere im Alter von 13-20 Monaten (weiß, Dreieck). Die Knochenaufnahme ist für das os petrosum aller Tiere dargestellt (schwarz, Viereck). (**B**) Korrelation der dynamischen 90 Minuten Messung (BPND) mit dem statisch berechneten Zeitfenster von 30 bis 60 Minuten, wobei die gepunktete Linie eine perfekte Übereinstimmung von 1 darstellt.

Weiterhin beobachteten wir eine deutliche longitudinale Progression in der Aufnahme von [^{18}F]-Florbetaben im frontalen Cortex der APP-Swe Mäuse im Gegensatz zu stabil bleibenden C57Bl/6 Tieren (**Abb.3**).

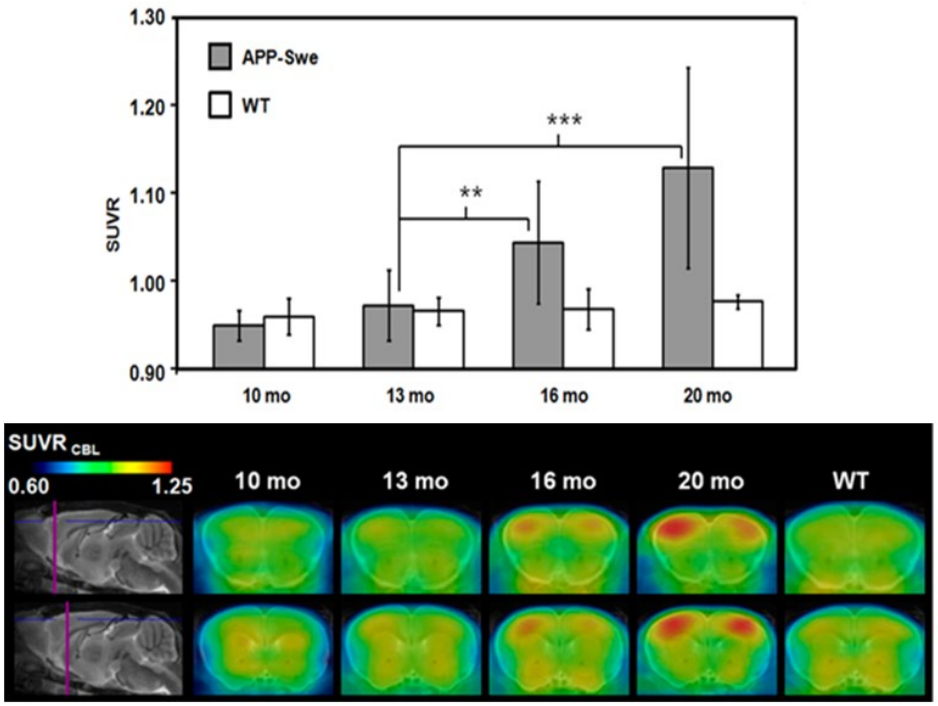

Abbildung 3: Longitudinale Änderungen im cortikalen Signal (SUVR ± Stabw.) in Gruppen von APP-Swe und C57Bl/6 (WT) Tieren im Alter von 10 (N = 5), 13 (N = 10), 16 (N = 8) und 20 Monaten (N = 5). Korrespondierende coronale Schnitte durch den frontalen Cortex sind auf einen MRT-Atlas des Mausgehirnes überlagert. ** kennzeichnet ein Signifikanzniveau von $p < 0.01$; *** kennzeichnet ein Signifikanzniveau von $p < 0.001$.

Hierzu wurden auch statistische parametrische voxel-basierte Vergleiche mittels SPM5 (Statistical Parametric Mapping; Wellcome Department of Cognitive Neurology) durchgeführt, um auch diskrete Veränderungen außerhalb der festgelegten Zielvolumina ebenfalls detektieren zu können. Kleinere Cluster mit signifikant höherer Traceraufnahme waren an dieser Stelle auch schon in 13 Monate alten APP-Swe Mäusen zu beobachten und zeigten die erhöhte Sensitivität der voxel-basierten Analysen (**Abb. 4**).

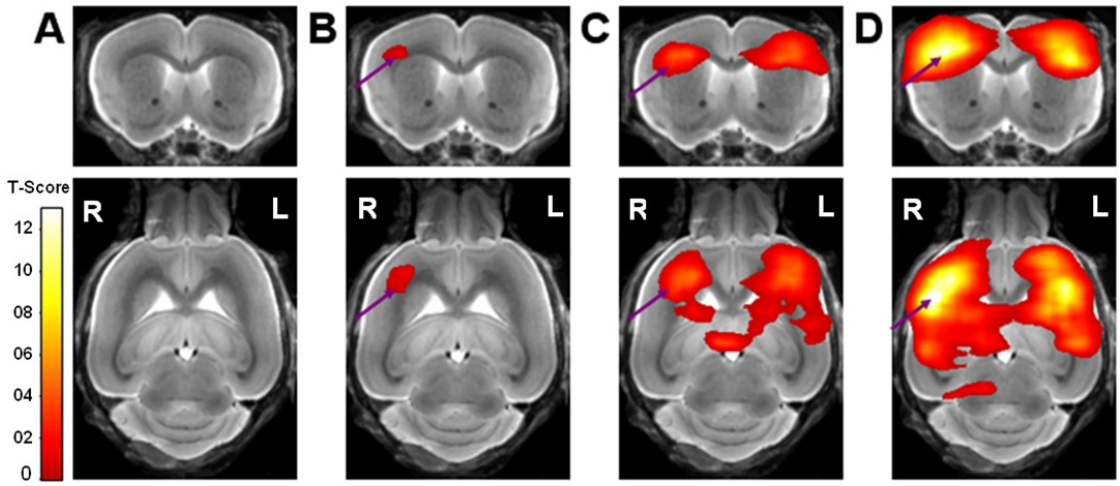

Abbildung 4: Voxel-basierte Analysen im Gruppenvergleich von APP-Swe Tieren im Alter von 10 (N = 5; **A**), 13 (N = 10; **B**), 16 (N = 8; **C**) und 20 Monaten (N = 5; **D**) jeweils mit aggregierten C57Bl/6 Tieren (10-20 Monate). Coronale (obere Reihe) und axiale (untere Reihe) Schnitte durch den Cortex sind auf einen MRT-Atlas des Mausgehirnes überlagert. Der T-Score kennzeichnet die Abweichung vom Kollektiv der C57Bl/6 Tiere. Lila Pfeile kennzeichnen einen frühen und zugleich stark progredienten Cluster.

Im Anschluss an die finalen PET Akquisitionen durchgeführte histologische Untersuchungen ergaben eine exzellente Korrelation ($R = 0.95$; $p < 0.001$) der Traceraufnahme mit der Menge (% Plaqueload) an durch Methoxy-X04 (Klunk, Bacskai et al. 2002) gefärbten ß-Amyloid Plaques. Zusammengefasst ließ sich festhalten, dass die Kombination aus Mausmodell, Radiotracer und der Auswertungsmethodik sowohl Robustheit als auch Verlässlichkeit bewies. Daraus konnten wir die Eignung des Modelles für longitudinale durch [^{18}F]-Florbetaben ß-Amyloid PET überwachte medikamentöse Interventionsstudien ableiten.

Diese Ergebnisse wurden im Rahmen meiner geteilten Erstautorschaft *"Longitudinal Assessment of Cerebral b-Amyloid Deposition in Mice Overexpressing Swedish Mutant ß-Amyloid Precursor Protein Using 18F-Florbetaben PET"* im Mai 2013 im Journal of Nuclear Medicine veröffentlicht.

2.2 Korrektur für Partialvolumeneffekte für das Gehirn der Maus

Dennoch gab es in der oben beschriebenen Validierungsstudie Diskrepanzen zwischen der Signalhöhe der Radiotraceraufnahme in der Auswertung von PET und Autoradiographie (exemplarische Subanalyse), die darauf hindeuteten, dass die Zunahme des gemessenen Signales unterschätzt wird. Auch eine andere ähnlich konfigurierte Kleintierstudie gelangte, unter Verwendung eines anderen Radiotracers und eines anderen Mausmodelles, zu ähnlichen Auffälligkeiten zwischen PET und Autoradiographie (Poisnel, Dhilly et al. 2012). Da vor allem die um ein Vielfaches höhere räumliche Ortsauflösung den Unterschied in der Auswertung der beiden Verfahren ausmacht, stellten wir die Hypothese auf, dass die beobachteten Diskrepanzen a.e. auf Partialvolumeneffekte zurückzuführen sind.

Im Rahmen meiner zweiten Erstautorschaft *"Impact of partial volume effect correction on cerebral β-amyloid imaging in APP-Swe mice using [18F]-florbetaben PET"* (Jan 2014, Neuroimage) setzte ich mich mit dieser Hypothese auseinander und konnte zeigen, dass eine Korrektur für Partialvolumeneffekte (PVEC) für das Gehirn der Maus sinnvoll anwendbar ist und zudem die Statistik in longitudinalen Vergleichen durch eine Erhöhung der Sensitivität stärkt.

Zunächst wurde durch ein Stabphantom eine präzise Erhebung der Halbwertsbreite (full-width-at-half-maximum, FWHM), als Maß für die Auflösung des Kleintier PET Scanners für den spezifischen Versuchsaufbau

inklusive der standardisierten Rekonstruktionsalgorithmen durchgeführt. Die FWHM wurde mit 1,72 mm berechnet und wurde in einer zweiten Phantomstudie zur Validierung eines für das humane Gehirn entwickelten PVEC Algorithmus (Rousset, Ma et al. 1998; Rousset, Collins et al. 2008) in den Dimensionen des Mausgehirnes verwendet. Hierfür wurde [^{18}F] in verschiedenen kreuzvalidierten Aktivitätshöhen in eine 96-Well-Platte gefüllt und analog der Akquisitions- und Rekonstruktionsalgorithmen zu APP-Swe/C57Bl/6 Mäusen gemessen und ausgewertet. Unkorrigierte Werte wiesen eine Unterschätzung von 14,2 - 24,3% auf, wohingegen durch PVEC eine Reduktion dieser Abweichung bis auf 3,1% erreicht werden konnte (**Abb. 5 A, B**). Bei Verwendung der experimentell bestimmten FWHM für den PVEC Algorithmus konnten die besten Übereinstimmungen mit den kreuzvalidierten Aktivitäten erreicht werden (**Abb. 5 C**).

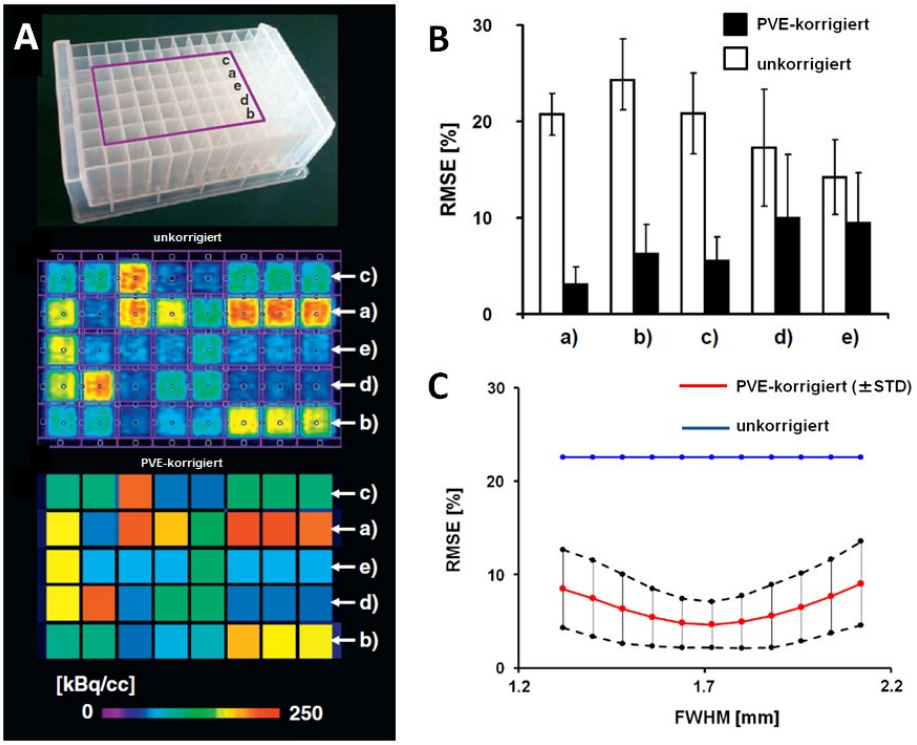

Abbildung 5: (**A**) Validierungs-Phantom für den PVEC Algorithmus. (**B**) Mittlerer quadratischer Fehler (RSME) [%] ± Stabw. für fünf verwendete Radioaktivitäts-Konzentrationen (a: 225,3; b: 182,7; c: 93,6; d: 61,3; e: 41,5 kBq/cc) der 96-Well-Platte in unkorrigierten (weiße Balken) und PVE-korrigierten (schwarze Balken; FWHM: 1,72

mm) Daten. (**C**) Die Korrektur mit abweichenden FWHM Parametern (± 5 Stabw.) für die beiden hohen Aktivitäten (a und b) zeigt geringere mittlere quadratische Fehler (RMSE) [%] (rote Linie) ± Stabw. (gestrichelte Linien) im Vergleich mit unkorrigierten Daten (blaue Linie) für die gesamte Bandbreite, aber die beste Übereinstimmung mit der im Stabphantom gemessenen FWHM.

Nach Konfigurierung zwölf verschiedener Masken mit zerebralen und extrazerebralen Anteilen wurden der frontale Cortex, das Kleinhirn und das restliche Gehirn von sechs C57Bl/6 Mäuse direkt nach einem [^{18}F]-Florbetaben PET Scan in Goldstandard Untersuchungen (Autoradiographie, Gamma-Counter) kreuzvalidiert. Auch hier zeigten sich deutliche Unterschätzungen der Aktivitätshöhe in den unkorrigierten PET Daten, wobei die besten Übereinstimmungen nach PVEC mit einer Maske inklusive extrazerebraler Kompartimente resultierten. Anschließend erfolgte die Translation auf die bestehenden longitudinalen [^{18}F]-Florbetaben Daten, wodurch die Diskrepanzen zwischen PET und Autoradiographie (18,9 ± 8,9%) deutlich reduziert werden konnten(4,8 ± 1,5%). Zudem ergab sich eine nicht lineare Korrekturfunktion (**Abb. 6A**) mit überproportional höher korrigierten $SUVR_{CTX/CBL}$ Werten in Tieren mit einer hohen cortikalen Amyloidose. Gruppenunterschiede berechneten sich durchgängig erhöht in korrigierten Daten (**Abb. 6B**).

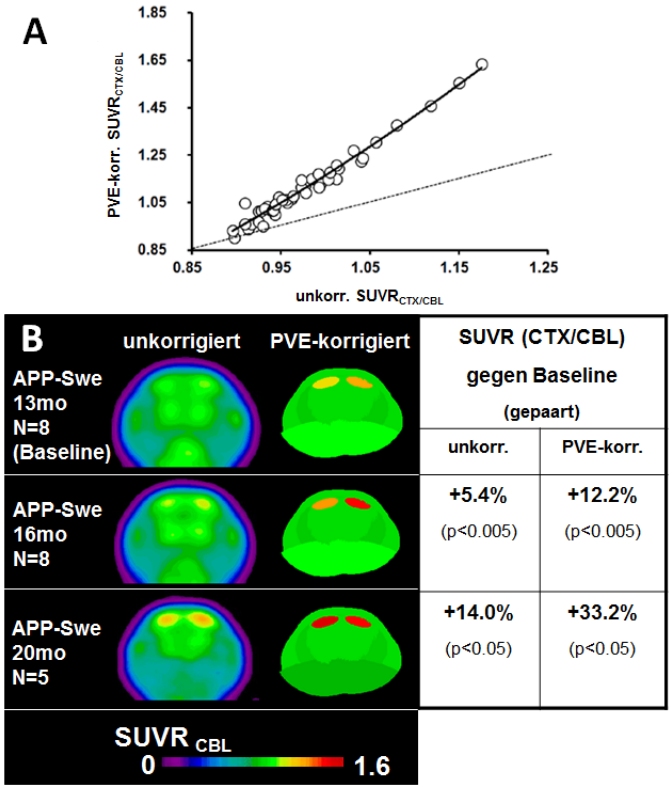

Abbildung 6: Funktionsgleichung der PVEC: $y = 1{,}16x^{2{,}04}$ (**A**), ermittelt durch das Auftragen der unkorrigierten und PVE-korrigierten $SUVR_{CTX/CBL}$ Werte unter Verwendung der Rohdaten der longitudinalen [^{18}F]-Florbetaben Studie. Prozentualer Einfluss der PVEC auf die longitudinalen Gruppenunterschiede über die Zeitspanne von 13 bis 20 Monaten (**B**) mit Visualisierung durch frontale coronale Schnitte in den entsprechenden APP-Swe Tieren.

Eine Extrapolation auf einen möglichen Therapieeffekt ergab zudem eine konsequent höhere statistische Power für Partialvolumeneffekt-korrigierte Daten (**Abb. 7**).

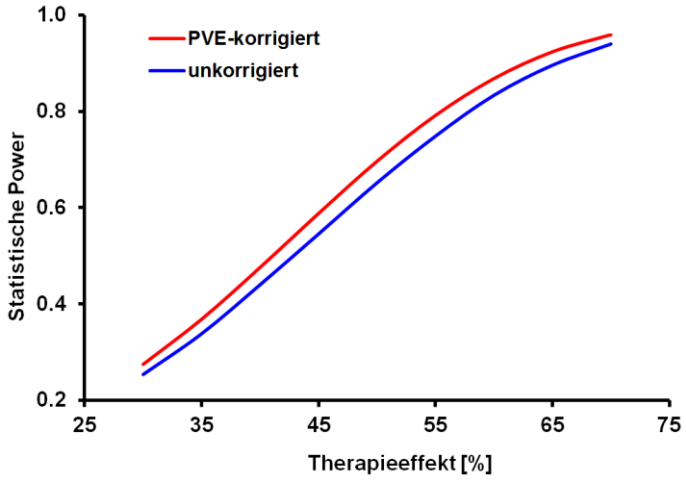

Abbildung 7: Power Kalkulation für longitudinale Vergleiche durch Extrapolation auf mögliche Therapieeffekte. Basierend auf gepaarten T-Tests zwischen APP-Swe Mäusen (N = 8; 13 und 16 Monate) ist die statistische Power für unkorrigierte (blaue Line) und PVE-korrigierte (rote Line) Daten dargestellt.

Insbesondere Tiere mit einer hohen cortikalen ß-Amyloid Manifestation, profitierten aufgrund der "Hot-Spot" Technik der ß-Amyloid PET von der Korrektur, da ein lokal hohes Signal in einem niedrigen Hintergrund überproportional durch Partialvolumeneffekte abgeschwächt wird. Somit konnten wir zeigen, dass durch die Anwendung einer PVEC zum einen deutlich akkuratere Quantifizierungen erzielt werden können und dass gerade longitudinale Interventionsstudien einen Benefit durch die Erhöhung der Sensitivität erlangen. Die Translation der validierten Methodik, unter Bezug auf den verwendeten VOI-basierten Algorithmus, auf andersartige Tiermodelle und Radiotracer erschien zudem überaus vielversprechend und ist das Gegenstand weiterer Studien.

3. Zusammenfassung

Ziel dieser Promotionsarbeit war es, eine longitudinale ß-Amyloid Positronen-Emissions-Tomographie (PET) im transgenen Mausmodell zu etablieren und validieren, um die Voraussetzungen für ein *in vivo* Monitoring neuer Therapieansätze bezüglich der Alzheimer Erkrankung zu schaffen. Bedingungen für die Einsetzbarkeit stellten zum einen die Erstellung und Validierung einer robusten Auswertemethodik dar. Zum anderen galt es, die Methodik unter dem Gesichtspunkt der kleinen Zielstrukturen in Bezug auf die vergleichsweise schlechte Auflösung der PET zu optimieren. Hierbei spielen Partialvolumeneffekte (PVE) eine große Rolle, so dass in einem zweiten Schritt diese systematisch analysiert wurden, um daraufhin einen anwendungsbezogenen Korrekturalgorithmus (PVEC) für das Gehirn der Maus zu validieren.

Im longitudinalen Verlauf wurden Gruppen von 10 bis 20 Monate alten transgenen APP-Swe Mäusen und altersgematchte C57Bl/6 Kontrolltiere nach einer Schwanzveneninjektion von 8,9 ± 2,7 MBq [^{18}F]-Florbetaben 90 Minuten lang dynamisch in einem Siemens Inveon Kleintier PET gemessen. Nach stereotaktischer Normalisierung der PET-Daten auf einen standardisierten MRT-Atlas des Mausgehirnes und Konfiguration von drei-dimensionalen Zielvolumina, wurden die PET Daten sowohl mittels kinetischem Modell (Logan; Bindungspotential) als auch in statischen Zeitfenstern (Standard-Aufnahme-Wert, SUV) ausgewertet; das Kleinhirn diente jeweils als pathologiefreie Referenzregion. Zusätzlich wurden parametrische voxel-basierte Auswertungen durchgeführt. Am Ende der Studie wurden die Gehirne histologisch und autoradiographisch aufbereitet und analysiert.

Für den zweiten Schritt, die Etablierung der PVEC, wurden Phantomstudien durchgeführt, um die exakte Halbwertsbreite (FWHM) des Kleintier PET Scanners zu ermitteln und einen Zielvolumen-basierten PVEC Ansatz validieren zu können. Mittels cortikalen Zielvolumen-Masken wurden unkorrigierte und PVE-korrigierte Daten von C57Bl/6 Mäusen erhoben und nach dem PET Scan gegen Gamma-Quanten-Messung und Autoradiographie kreuzvalidiert. Anschließend wurde der Algorithmus auf den longitudinalen Datensatz angewendet, um den Effekt der PVEC zu analysieren und die statistische Teststärke zwischen unkorrigierten Daten und PVE-korrigierten Daten zu vergleichen.

In der longitudinalen Studie konnte ein statisches 30 – 60 Minuten p.i. Zeitfenster identifiziert werden, welches die beste Übereinstimmung mit dem kinetischen Modell (Logan, 90 Minuten) zeigte. Gegenüber der Baseline (13 Monate) wiesen APP-Swe Mäuse einen Anstieg des cortikalen PET Signales im Alter von 16 Monaten (+7,9%, $p < 0,01$) sowie 20 Monaten (+16,6%, $p < 0,001$) auf. In C57Bl/6 Kontrolltieren zeigten sich keine signifikanten longitudinalen Veränderungen, bei ähnlicher Signalintensität wie in 10 oder 13 Monate alten transgenen Tieren. Durch die voxel-basierten Gruppenvergleiche konnten Cluster mit einem signifikant erhöhten ß-Amyloid Level im frontalen Cortex ($p < 0,001$) in APP-Swe Tieren auch schon im Alter von 13 Monaten detektiert werden, welche daraufhin eine fronto-temporale Progredienz bis zum Alter von 20 Monaten entwickelten. Die histologischen Analysen mit der Methoxy-X04 Färbung für fibrilläres ß-Amyloid ergaben eine hervorragende Übereinstimmung mit dem PET Signal ($R = 0,95$; $p < 0,001$). Autoradiographisch analysierte Hirnschnitte zeigten deutlich höhere Cortex-zu-Kleinhirn-Werte als die korrespondierenden *in vivo* PET

Ergebnisse, wobei PVE als wahrscheinlichste Quelle der Diskrepanz angenommen wurden.

Im Rahmen der Phantomstudien konnte eine FWHM von 1,72 mm für den Kleintier PET Scanner mit dem dezidierten Versuchsaufbau ermittelt werden. Dadurch konnten mit der Zielvolumen-basierten PVEC valide und reproduzierbare Ergebnisse erzielt werden. Unter Verwendung einer Zielvolumen-Maske inklusive extra-cortikaler Regionen konnte in der Kreuzvalidierung des PET Signales die beste Übereinstimmung mit der Gamma-Quanten-Messung und der Autoradiographie erreicht werden. Im gepaarten Vergleich der longitudinalen Ergebnisse in APP-Swe Mäusen zeigte sich in PVE-korrigierten Daten eine Zunahme von 12,2% ($p < 0,05$; 16 Monate) und 36,4% ($p < 0,005$; 20 Monate) gegenüber der Baseline bei 13 Monaten. In unkorrigierten Daten resultierten diese Unterschiede bei 5,5% ($p < 0,05$; 16 Monate) und 15,5% ($p < 0,005$; 20 Monate). Die prozentuale Abweichung zwischen PET Signal und Autoradiographie konnte von -18,9% (unkorrigiert) auf -4,8% (PVEC) verringert werden, bei gleichbleibend guter Korrelation mit der Histologie. Durch die Extrapolation auf mögliche Therapieeffekte konnte gezeigt werden, dass die Anwendung der PVEC die statistische Teststärke zur Detektion von longitudinalen Gruppenunterschieden zwischen therapierten und nicht therapierten Tieren um ca. 10% erhöht.

Das APP-Swe Mausmodell stellt in Verbindung mit der [^{18}F]-Florbetaben Kleintier PET eine valide und robuste Methodik dar, um Therapieeffekte potenzieller anti-amyloidogener Therapiesubstanzen *in vivo* monitoren zu können. Eine Ökonomisierung im Sinne einer kürzeren PET Akquisitionsdauer konnte durch ein statisches 30 Minuten Zeitfenster

erreicht werden. Die PVEC beim Maushirn stellt eine sinnvolle Möglichkeit dar, um die limitierte Ortsauflösung der PET auszugleichen und Abweichungen des PET Signales von Goldstandard-Untersuchungen signifikant zu verringern. Weiterhin kann die Anwendung einer PVEC dazu beitragen, Therapieeffekte sensitiver zu detektieren.

4. Summary

The aim of this doctoral thesis was to establish longitudinal ß-amyloid positron emission tomography (PET) in a transgenic mouse model, meeting the criteria for *in vivo* monitoring of novel therapeutic approaches to Alzheimer's disease. Requirements for such a model were the generation and validation of a robust and feasible PET analysis method, optimized with regard to the inherently low spatial resolution of PET in relation to the mouse brain. Partial volume effects (PVE) play a major role to the distortion of PET signals, leading us to undertake a fundamental investigation of the magnitude of PVE at the scale of small animal PET imaging. Furthermore, we established for the first time a PVE correction algorithm (PVEC) for the mouse brain, using a volume-of-interest (VOI) based approach.

Groups of transgenic APP-Swe mice aged 10 to 20 months and age-matched C57Bl/6 littermates were longitudinally imaged using a dedicated Siemens Inveon small animal PET, initially with dynamic 90 minute emission recordings beginning upon injection of the ß-amyloid tracer [^{18}F]-Florbetaben (8.9 ± 2.7 MBq) to a tail vein. Stereotactic normalization of summation images to a standard MRI mouse brain template and volume of interest (VOI) segmentation was followed by kinetic analysis (Logan reference tissue binding potential) and static frame analyses (standard-uptake-value-ratios, SUVR), both using the cerebellum as a reference region with absence of pathology. Voxel-wise analyses of PET results were contrasted by statistical parametric mapping (SPM). Histological analyses and *ex vivo* autoradiography were ultimately performed in a subset of animals as gold standard assessments of ß-amyloid accumulation.

Phantom studies were performed to estimate the most precise full-width-at-half-maximum (FWHM) of the small animal PET scanner and to validate a VOI-based PVEC method. Several VOI-brain masks were used for cross-validation of uncorrected and PVE-corrected PET data recorded from C57Bl/6 mice, with gamma-counter and autoradiography assessments, which are unaffected by PVE. Furthermore, the correction algorithm was applied to a longitudinal study of transgenic mice (APP-Swe), for verifying the improved quantitation of ß-amyloid through PVEC, and to compare the statistical power of uncorrected and PVE-corrected PET data.

The 30 to 60 minute time frame proved suitable for further analyses, based on agreement with the 90 minute kinetic assessment. APP-Swe mice revealed an increase in cortical [^{18}F]-florbetaben uptake at 16 months (+7.9%, $p < 0.01$), which progressed to 20 months (16.6%, $p < 0.001$) relative to baseline findings at 13 months. Relative to findings in C57Bl/6 control mice, there was no discernible increase in cortical tracer uptake at 10 and 13 months in APP-Swe animals. Voxelwise group comparisons yielded clusters of significantly higher ß-amyloid levels ($p < 0.001$) in frontal cortex of the APP-Swe mice as early as 13 months, which showed further fronto-temporal progression until the age of 20 months. Methoxy-X04 staining for fibrillar ß-amyloid had excellent correlation with the PET signal ($R = 0.95$; $p < 0.001$), whereas autoradiographic analysis of brain slices collected ex vivo revealed higher cortex-to-cerebellum ratios than was evident in the corresponding PET images; we attribute this bias to PVE.

Phantom studies indicated a FWHM of 1.72 for the small animal PET scanner, and supported the validity and reliability for the VOI-based PVEC approach. Applying a VOI-brain mask also including extracerebral structures

proved the best agreement in cross-validation with gamma-counter and autoradiography assessments. Paired longitudinal comparisons of APP-Swe mice using PVE-corrected data revealed an increase of ß-amyloid levels by 12.2% ($p < 0.05$; 16 months) and 36.4% ($p < 0.005$; 20 months) relative to the 13 month baseline. Corresponding uncorrected PET data showed increases of only 5.5% ($p < 0.05$; 16 months) and 15.5% ($p < 0.005$; 20 months). The discrepancies between PET signal and autoradiography were reduced from -18.9% (uncorrected) to -4.8% (PVE-corrected), in consistently good correlation with histology. Extrapolation of possible treatment effects showed a 10% increase in statistical power increase for the detection of longitudinal group differences between treated and untreated animals when using PVEC.

Small animal [^{18}F]-florbetaben ß-amyloid PET in conjunction with APP-Swe mice offers a valid and robust method for *in vivo* monitoring of potential novel disease modifying approaches to the treatment of Alzheimer´s disease. We found that shortening the PET acquisition time to a single 30 minute time frame affords a considerable economy in data acquisition, without penalty in sensitivity of the method for ß-amyloid quantitation. PVEC for the mouse brain accommodates the low spatial resolution of PET, and significantly reduces deviations of PET findings relative to gold standard autoradiography assessment. Thus, routine implementation of mouse brain PVEC will increase the sensitivity of ß-amyloid PET for detection of therapy effects in future studies.

5. Literaturverzeichnis

Barthel, H. and O. Sabri (2011). "Florbetaben to trace amyloid-beta in the Alzheimer brain by means of PET." J Alzheimers Dis **26 Suppl 3**: 117-121.

Cheng, J. C., K. Shoghi, et al. (2012). "Quantitative accuracy of MAP reconstruction for dynamic PET imaging in small animals." Med Phys **39**(2): 1029-1041.

Clark, C. M., J. A. Schneider, et al. (2011). "Use of florbetapir-PET for imaging beta-amyloid pathology." JAMA **305**(3): 275-283.

Coric, V., C. H. van Dyck, et al. (2012). "Safety and tolerability of the gamma-secretase inhibitor avagacestat in a phase 2 study of mild to moderate Alzheimer disease." Arch Neurol **69**(11): 1430-1440.

Fleisher, A. S., R. Raman, et al. (2008). "Phase 2 safety trial targeting amyloid beta production with a gamma-secretase inhibitor in Alzheimer disease." Arch Neurol **65**(8): 1031-1038.

Green, R. C., L. S. Schneider, et al. (2009). "Effect of tarenflurbil on cognitive decline and activities of daily living in patients with mild Alzheimer disease: a randomized controlled trial." JAMA **302**(23): 2557-2564.

Klunk, W. E., B. J. Bacskai, et al. (2002). "Imaging Abeta plaques in living transgenic mice with multiphoton microscopy and methoxy-X04, a systemically administered Congo red derivative." J Neuropathol Exp Neurol **61**(9): 797-805.

Klunk, W. E., H. Engler, et al. (2004). "Imaging brain amyloid in Alzheimer's disease with Pittsburgh Compound-B." Ann Neurol **55**(3): 306-319.

Kuntner, C., A. L. Kesner, et al. (2009). "Limitations of small animal PET imaging with [18F]FDDNP and FDG for quantitative studies in a transgenic mouse model of Alzheimer's disease." Mol Imaging Biol **11**(4): 236-240.

LaFerla, F. M. (2010). "Pathways linking Abeta and tau pathologies." Biochem Soc Trans **38**(4): 993-995.

Lehnert, W., M. C. Gregoire, et al. (2012). "Characterisation of partial volume effect and region-based correction in small animal positron emission tomography (PET) of the rat brain." Neuroimage **60**(4): 2144-2157.

Maeda, J., B. Ji, et al. (2007). "Longitudinal, quantitative assessment of amyloid, neuroinflammation, and anti-amyloid treatment in a living mouse model of Alzheimer's disease enabled by positron emission tomography." J Neurosci **27**(41): 10957-10968.

Manook, A., B. H. Yousefi, et al. (2012). "Small-animal PET imaging of amyloid-beta plaques with [11C]PiB and its multi-modal validation in an APP/PS1 mouse model of Alzheimer's disease." PLoS One **7**(3): e31310.

Nandoe Tewarie, R. D., J. Yu, et al. (2010). "Positron emission tomography for serial imaging of the contused adult rat spinal cord." Mol Imaging **9**(2): 108-116.

Oakley, H., S. L. Cole, et al. (2006). "Intraneuronal beta-amyloid aggregates, neurodegeneration, and neuron loss in transgenic mice with five familial Alzheimer's disease mutations: potential factors in amyloid plaque formation." J Neurosci **26**(40): 10129-10140.

Palop, J. J. and L. Mucke (2010). "Amyloid-beta-induced neuronal dysfunction in Alzheimer's disease: from synapses toward neural networks." Nat Neurosci **13**(7): 812-818.

Poisnel, G., M. Dhilly, et al. (2012). "PET imaging with [18F]AV-45 in an APP/PS1-21 murine model of amyloid plaque deposition." Neurobiol Aging.

Richards, J. G., G. A. Higgins, et al. (2003). "PS2APP transgenic mice, coexpressing hPS2mut and hAPPswe, show age-related cognitive deficits associated with discrete brain amyloid deposition and inflammation." J Neurosci **23**(26): 8989-9003.

Rominger, A., E. Mille, et al. (2010). "Validation of the octamouse for simultaneous 18F-fallypride small-animal PET recordings from 8 mice." J Nucl Med **51**(10): 1576-1583.

Rousset, O. G., D. L. Collins, et al. (2008). "Design and implementation of an automated partial volume correction in PET: application to dopamine receptor quantification in the normal human striatum." J Nucl Med **49**(7): 1097-1106.

Rousset, O. G., Y. Ma, et al. (1998). "Correction for partial volume effects in PET: principle and validation." J Nucl Med **39**(5): 904-911.

Schenk, D., G. S. Basi, et al. (2012). "Treatment strategies targeting amyloid beta-protein." Cold Spring Harb Perspect Med **2**(9): a006387.

Schneider, L. S. (2013). "Alzheimer disease pharmacologic treatment and treatment research." Continuum (Minneap Minn) **19**(2 Dementia): 339-357.

Teipel, S. J., R. Buchert, et al. (2011). "Development of Alzheimer-disease neuroimaging-biomarkers using mouse models with amyloid-precursor protein-transgene expression." Prog Neurobiol.

Toyama, H., M. Ichise, et al. (2004). "Evaluation of anesthesia effects on [18F]FDG uptake in mouse brain and heart using small animal PET." Nucl Med Biol **31**(2): 251-256.

Toyama, H., D. Ye, et al. (2005). "PET imaging of brain with the beta-amyloid probe, [11C]6-OH-BTA-1, in a transgenic mouse model of Alzheimer's disease." Eur J Nucl Med Mol Imaging **32**(5): 593-600.

Vandenberghe, R., K. Van Laere, et al. (2010). "18F-flutemetamol amyloid imaging in Alzheimer disease and mild cognitive impairment: a phase 2 trial." Ann Neurol **68**(3): 319-329.

Villemagne, V. L., S. Burnham, et al. (2013). "Amyloid beta deposition, neurodegeneration, and cognitive decline in sporadic Alzheimer's disease: a prospective cohort study." Lancet Neurol **12**(4): 357-367.

Visser, E. P., J. A. Disselhorst, et al. (2009). "Spatial resolution and sensitivity of the Inveon small-animal PET scanner." J Nucl Med **50**(1): 139-147.

Visser, P. J., H. Wolf, et al. (2012). "Disclosure of Alzheimer's disease biomarker status in subjects with mild cognitive impairment." Biomark Med **6**(4): 365-368.

Wolfe, M. S. (2012). "gamma-Secretase as a target for Alzheimer's disease." Adv Pharmacol **64**: 127-153.

Yu, Y., V. Logovinsky, et al. (2013). "Safety, tolerability, pharmacokinetics, and pharmacodynamics of the novel gamma-secretase modulator, E2212, in healthy human subjects." J Clin Pharmacol.

Ziegler-Graham, K., R. Brookmeyer, et al. (2008). "Worldwide variation in the doubling time of Alzheimer's disease incidence rates." Alzheimers Dement **4**(5): 316-323.

6. Danksagung

Meinem Doktorvater, Herrn PD Dr. med. Axel Rominger von der Klinik und Poliklinik für Nuklearmedizin der Universität München danke ich für die Überlassung des Themas und der Betreuung dieser Arbeit. Die freundschaftliche und produktive Zusammenarbeit war stets angenehm, immer konstruktiv und mündete in vielversprechende Projekte, weit über diese Dissertation hinaus.

Herrn Prof. Dr. med. Peter Bartenstein möchte ich für die Initiierung des Projektes und die Knüpfung der Kooperationen danken.

Andreas Delker und Guido Böning danke ich für die physikalische Beratung und Durchführung bei den Phantommessungen und die Vermittlung des Verständnisses für die PET Methodik. Andrei Todica, Harun Ilhan und Erik Mille gilt mein Dank für die kompetente Unterstützung im Bezug auf die gesamte Software und Auswertemethodik und vor allem für viele interessante Stunden im Doktorandenraum. Meiner Nachfolgerin Christina Rötzer danke ich für die Unterstützung und vor allem ihrem Fleiß bei den finalen Versuchen.

Weiterhin danke ich Heidrun Zankl, Rosel Oos, Karin Bormann-Giglmaier und Matthias Mooser für die exzellente methodische und technische Unterstützung und die hervorragende Zusammenarbeit bei der Durchführung der Experimente.

Für das Ermöglichen des Studiums und die herzliche Unterstützung gilt mein tiefer Dank meiner Mutter.

Ganz besonders möchte ich mich bei meiner Verlobten Eva bedanken, die sich oft wilde Theorien und Ideen schon beim Frühstück anhören musste und mir trotzdem immer mit Geduld und Rat zur Seite stand.

Journal of Nuclear Medicine, published on May 31, 2013 as doi:10.2967/jnumed.112.114660

Longitudinal Assessment of Cerebral β-Amyloid Deposition in Mice Overexpressing Swedish Mutant β-Amyloid Precursor Protein Using ^{18}F-Florbetaben PET

Axel Rominger*[1], Matthias Brendel*[1], Steffen Burgold[2], Kevin Keppler[2], Karlheinz Baumann[3], Guoming Xiong[1], Erik Mille[1], Franz-Josef Gildehaus[1], Janette Carlsen[1], Juli Schlichtiger[1], Sabrina Niedermoser[1], Björn Wängler[1], Paul Cumming[4], Harald Steiner[5,6], Jochen Herms[2], Christian Haass[5–7], and Peter Bartenstein[1,7]

[1]Department of Nuclear Medicine, Ludwig-Maximilians-University of Munich, Munich, Germany; [2]Department of Translational Brain Research, German Center for Neurodegenerative Diseases (DZNE) Munich, Ludwig-Maximilians-University of Munich, Munich, Germany; [3]F. Hoffmann-La Roche AG, pRED, Pharma Research and Early Development, DTA CNS, Basel, Switzerland; [4]ABX, Radeberg, Germany; [5]Adolf-Butenandt-Institute, Biochemistry, Ludwig-Maximilians-University of Munich, Munich, Germany; [6]German Center for Neurodegenerative Diseases (DZNE), Munich, Germany; and [7]Munich Cluster for Systems Neurology (SyNergy), Munich, Germany

The progression of β-amyloid deposition in the brains of mice overexpressing Swedish mutant β-amyloid precursor protein (APP-Swe), a model of Alzheimer disease (AD), was investigated in a longitudinal PET study using the novel β-amyloid tracer ^{18}F-florbetaben. **Methods:** Groups of APP-Swe and age-matched wild-type (WT) mice (age range, 10–20 mo) were investigated. Dynamic emission recordings were acquired with a small-animal PET scanner during 90 min after the administration of ^{18}F-florbetaben (9 MBq, intravenously). After spatial normalization of individual PET recordings to common coordinates for mouse brain, binding potentials (BP_{ND}) and standardized uptake value ratios (SUVRs) were calculated relative to the cerebellum. Voxelwise analyses were performed using statistical parametric mapping (SPM). Histochemical analyses and ex vivo autoradiography were ultimately performed in a subset of animals as a gold standard assessment of β-amyloid plaque load. **Results:** SUVRs calculated from static recordings during the interval of 30–60 min after tracer injection correlated highly with estimates of BP_{ND} based on the entire dynamic emission recordings. ^{18}F-florbetaben binding did not significantly differ in APP-Swe mice and WT animals at 10 and 13 mo of age. At 16 mo of age, the APP-Swe mice had a significant 7.9% increase ($P < 0.01$) in cortical ^{18}F-florbetaben uptake above baseline and at 20 mo there was a 16.6% increase ($P < 0.001$), whereas WT mice did not show any temporal changes in tracer uptake during the interval of follow-up. Voxelwise SPM analyses revealed the first signs of increased cortical binding at 13 mo and confirmed progressive binding increases in both the frontal and the temporal cortices ($P < 0.001$ uncorrected) to 20 mo. The SUVR strongly correlated with percentage plaque load ($R = 0.95$, $P < 0.001$). **Conclusion:** In the first longitudinal PET study in an AD mouse model using the novel β-amyloid tracer ^{18}F-florbetaben, the temporal and spatial progression of amyloidogenesis in the brain of APP-Swe mice were sensitively monitored. This method should afford the means for preclinical testing of novel therapeutic approaches to the treatment of AD.

Received Sep. 24, 2012; revision accepted Jan. 23, 2013.
For correspondence or reprints contact: Axel Rominger, Department of Nuclear Medicine, University of Munich, Marchioninistrasse 15, 81377 Munich, Germany.
E-mail: axel.rominger@med.uni-muenchen.de
*Contributed equally to this work.
Published online ■■■■.

Key Words: Alzheimer disease; β-amyloid plaque load; small-animal PET; transgenic mouse model; ^{18}F-florbetaben

J Nucl Med 2013; 54:1–8
DOI: 10.2967/jnumed.112.114660

Alzheimer disease (AD) is the most common form of dementia, with exponentially increasing incidence as a function of age among the elderly, which is imposing an onerous burden on health care in societies with aging populations (*1*). There is an urgent need to find biomarkers to predict future clinical decline and likewise for use as outcome measures in clinical trials of innovative disease-modifying agents (*2*). The main neuropathologic features of AD, which include the accumulation of extracellular β-amyloid plaques and intracellular neurofibrillary tangles (*3*), are emulated in transgenic animal models for AD (*4,5*). Although current transgenic AD models obviously do not manifest all clinical and pathologic aspects of AD (*6*), they are nonetheless of heuristic value for the testing of interventions that address certain aspects of the disease, notably the formation of β-amyloid plaques. In this regard, molecular imaging of β-amyloid by PET has emerged as an important endpoint for assessing the extent of disease progression, although only limited imaging data are available in rodent AD models (*7–11*). The β-amyloid ligand ^{18}F-florbetaben, with high affinity for fibrillary β-amyloid in vitro, is currently in clinical development by Bayer Healthcare and Piramal Imaging (*12–14*) and has proven to have high sensitivity and specificity in clinical PET examinations for distinguishing AD patients from healthy control subjects (*15*). However, the applicability of this agent for monitoring in longitudinal studies the accumulation of fibrillary β-amyloid in AD mice remains to be established.

The aim of this longitudinal PET study was to investigate the novel amyloid tracer ^{18}F-florbetaben in the transgenic APP-Swe mouse model, which expresses the Swedish double-mutation of the amyloid precursor protein (APP). We performed sequential ^{18}F-florbetaben PET examinations in groups of transgenic and wild-type (WT) mice (age range, 10–20 mo) and examined different approaches to quantitation of the β-amyloid signal in the brain. In

TABLE 1
Demographics, Overview of Modalities, and Results

Mouse strain	Sex	Age (mo)	Weight (g)	Drop-out due to death at or after PET scan (*n*)	PET scan successful (*n*)	Hemispheres (*n*)		PET		β-Amyloid plaque load (%)	Autoradiography cortex-to-cerebellum ratio
						Histochemistry	Autoradiography	SUVR	BP_{ND}		
APP-Swe	M	10	28.5 ± 3.9	3	5			0.95 ± 0.02	−0.05 ± 0.02		
		13	28.9 ± 3.9		2	2	2	0.94 ± 0.03	−0.04 ± 0.03	0.35 ± 0.41	1.03 ± 0.04
C57BL/6 (WT)	M	10	35.0 ± 1.9	1	5			0.96 ± 0.02	−0.03 ± 0.02		
		13	42.5 ± 4.2*		2			0.97 ± 0.02	−0.03 ± 0.02		
APP-Swe	F	13	26.7 ± 2.4		10			0.97 ± 0.03	−0.03 ± 0.04		
		16	26.7 ± 1.8	3	8			1.04 ± 0.07†	0.04 ± 0.07*		
		20	27.6 ± 2.3	2	5	8	2	1.13 ± 0.11‡	0.10 ± 0.11†	4.06 ± 2.78	1.51 ± 0.18
C57BL/6 (WT)	F	13	25.4 ± 1.6	2	8			0.97 ± 0.02	−0.03 ± 0.02		
		16	25.5 ± 0.9		8			0.97 ± 0.02	−0.03 ± 0.03		
		20	26.4 ± 2.5		6	2	2	0.98 ± 0.01	−0.02 ± 0.02	0	0.98 ± 0.02

*$P < 0.05$, 2-sample *t* test.
†$P < 0.01$, 2-sample *t* test.
‡$P < 0.001$, 2-sample *t* test.
Pilot (male mice; 10–13 mo) and main study (female mice; 13–20 mo); heterozygous APP-Swe mice and age- and sex-matched C57BL/6 (control group) mice were used. Data are mean ± SD.

addition, the PET results were validated in a subset of animals relative to findings by autoradiography ex vivo and histochemistry.

MARTERIALS AND METHODS

Radiochemistry

The ^{18}F-florbetaben precursor provided by Bayer Pharma AG was radiolabeled via the method of Zhang et al. (*12*), with slight modifications. The detailed description of this radiosynthesis is presented in the supplemental data (supplemental materials are available online only at http://jnm.snmjournals.org). This procedure yields a radiochemical purity exceeding 98% and specific activity of 80 GBq/μmol at the end of synthesis.

Animals

All experiments were performed in compliance with the National Guidelines for Animal Protection, Germany, and the approval of the animal care committee. Transgenic mice overexpressing human APP with the Swedish double mutation (K670N, M671L) driven by the mouse Thy1.2 promoter were generated as described earlier (*16*). These APP-Swe mice were backcrossed to C57BL/6 mice to generate a line with less than 5% DBA2 background (as determined by microsatellites genotyping). Mice heterozygous for the transgene start to accumulate β-amyloid at the age of approximately 9 mo and develop β-amyloid plaques around the age of 12 mo, mainly in the cortical mantle. At 18 mo of age, numerous amyloid plaques positively stained with Congo red are observed through the brains of these animals (Karlheinz Baumann, personal communication).

In the pilot study, 5 male heterozygous APP-Swe mice from Hoffmann-La Roche and 5 male C57BL/6 control mice purchased from Charles River Laboratories were investigated by molecular imaging. For the main study, 10 female heterozygous APP-Swe mice and 10 female age-matched C57BL/6 mice were used. Animals were housed in a temperature- and humidity-controlled environment with a 12-h light–dark cycle, with free access to food (Ssniff) and water.

Study Design

The study design entailed a longitudinal series of PET sessions at different ages. A detailed overview of the design is provided in Table 1. [**Table 1**]

Pilot Study Phase. PET recordings were obtained in 5 male transgenic and 5 male WT mice at the age of 10 and 13 mo; in 2 of these animals, autoradiography ex vivo and histochemistry were performed immediately after the final PET session

Main Study Phase. PET recordings were obtained in 10 female transgenic and 10 female WT mice at the age of 13, 16, and 20 mo, in conjunction with ex vivo autoradiography in 2 transgenic and 2 WT animals at 20 mo of age. Histochemistry was performed in all surviving transgenic animals at 20 mo.

PET Recordings: Data Acquisition

Mice were anesthetized with isoflurane (1.5%, delivered at 3.5 L/min) and placed in the aperture of the Siemens Inveon DPET as described previously (*17*). On injection of 8.9 ± 2.7 MBq of ^{18}F-florbetaben in 150 μL of saline to a tail vein, a 90-min dynamic emission recording was initiated, followed by a 15-min transmission scan using a rotating ^{57}Co point source. The dynamic acquisition protocol consisted of 19 frames (3 × 10, 1 × 30, 4 × 60, 5 × 300, and 6 × 600 s). After recovery from anesthesia, mice were returned to their home cages. In the case of terminal experiments,

jnm114660-pm ■ 5/24/13

animals were killed by cervical dislocation while still deeply anesthetized, before rapid removal of the brain. In the pilot study, an additional dynamic PET recording with ^{18}F-FDG (11.4 ± 0.2 MBq) lasting 15 min was obtained after the completion of the ^{18}F-florbetaben scan, without the mouse being removed from the scanner. The reconstructed ^{18}F-FDG emission image was used to facilitate a precise manual coregistration of ^{18}F-florbetaben scans in the pilot study, but this measure was otherwise deemed uninformative for the main study.

Image Reconstruction and PET Data Analyses

Reconstruction was performed with 3-dimensional ordered-subset expectation maximization and 3-dimensional maximum a posteriori (4 and 32 iterations, respectively); a zoom factor of 1.0; and scatter, attenuation, and decay correction, resulting in a final voxel dimension of 0.78 × 0.78 × 0.8 mm. A ^{18}F-florbetaben template was generated by coregistration of the ^{18}F-FDG and ^{18}F-florbetaben summation images to a mouse brain MR imaging atlas (*18*) using the PMOD fusion tool (version 3.302; PMOD Technologies Ltd.). A total-body volume of interest (VOI) was drawn to quantify the injected dose. Both VOI- and voxel-based analyses were performed after manual rigid-body coregistration and accurate alignment by manual reregistration of individual ^{18}F-florbetaben summation images on the ^{18}F-florbetaben template. For the purpose of quality control of the PET/MR image–fusion process, longitudinal PET data of individual mice were checked for exact overlapping so as to guarantee the best possible intraindividual coregistrations.

A cerebellar VOI comprising 36 mm^3, a frontal cortex VOI comprising 19 mm^3, and a hippocampal VOI comprising 9 mm^3 were designed so as to minimize signal loss due to partial-volume [**Fig. 1**] effects (Fig. 1) (*11,19*). The binding potential (BP_{ND}) was calculated voxelwise in the cortical VOI from the entire dynamic recordings using a linear graphic method (*20*), with the cerebellum serving as the reference tissue. The ^{18}F-florbetaben standardized uptake value ratio (SUVR) was calculated voxelwise and in the cortical VOI using different static time frames between 20 and 90 min after injection. For whole-brain voxelwise comparisons between groups of transgenic and WT mice, statistical parametric mapping (SPM) was performed using SPM5 routines (Wellcome Department of Cognitive Neurology) implemented in MATLAB (version 7.1; MathWorks Inc.), adapted from Sawiak et al. (*21*) for mouse data.

Ex Vivo Autoradiography

Autoradiography ex vivo was performed immediately after the ^{18}F-florbetaben PET scanning. A detailed description of the procedure is provided in the supplemental data. Resulting images were analyzed with AIDA image-analyzing software (version 4.50; Raytest GmbH). Each value was normalized with respect to the cerebellum as the control brain region (ratio to cerebellum).

Histochemistry: Acquisition and Image Analysis

A detailed description of the histochemistry acquisition procedure is provided in the supplemental data. For image analysis, we defined a region corresponding to the frontal cortex VOI from PET image analysis. The 3-dimensional image stacks were maximum-intensity-projected. The area and number of plaques were automatically counted in segmented images using Imaris software (Imaris 7.4.2; Bitplane). The corresponding volume for each plaque was calculated from the plaque area, assuming spheric plaques. Plaque load was calculated by integrating the volume of all plaques and relating it to the imaged volume. All experiments were performed in a manner blind to the results of PET analysis.

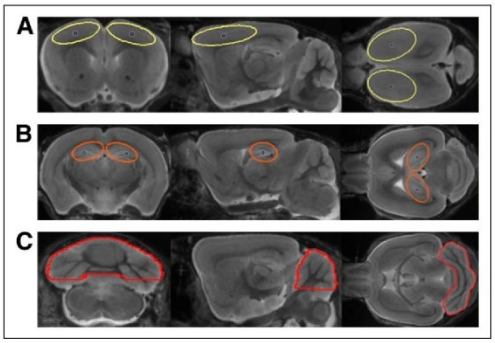

FIGURE 1. Definitions of cortical (yellow) (A), hippocampal (orange) (B), and cerebellar (red) (C) VOIs in mouse brain MR imaging atlas (*18*) in coronal, sagittal, and axial slices.

Statistics

Group comparisons of VOI-based PET results in transgenic versus WT mice were performed with the 2-sample Student *t* test using IBM SPSS Statistics (version 20.0; SPSS). For correlation analyses, Pearson coefficients of correlation (*R*) were calculated. A threshold of *P* less than 0.05 was considered to be significant for rejection of the null hypothesis. For the voxelwise group comparison (SPM5) of transgenic versus WT mice, 2-sample *t* tests were performed, with a significance threshold of *P* less than 0.001, uncorrected for multiple comparisons.

RESULTS

Animals

During the pilot and main studies, 58 PET scans were acquired in up to 3 sessions per animal. The drop-out rate was 20.1% per/after scan session, mainly because of the high sensitivity of the transgenic animals to prolonged intervals of anesthesia. No significant sex differences were observed with regard to quantitation; therefore, pilot and main study results at 13 mo were combined. The weight of male WT animals in the pilot study increased with age, whereas the weight for all female animals remained constant over time. All details of animal characteristics are displayed in Table 1.

Methodology and VOI-Based Analyses

Mean (±SD) target-to-cerebellum ratios in transgenic mice aged 13 and 20 mo and for pooled WT mice aged 10–20 mo, along with corresponding petrous bone-to-cerebellum ratios, are shown in Figure 2A. For illustrative purposes of extracerebral [**Fig. 2**] activity, serial PET recordings from different time frames are depicted in Figure 2B, and a cerebellum reference tissue Logan plot for the cortical VOI in 20-mo-old transgenic animals is presented in Figure 2C. The time–activity curves suggest the attainment of equilibrium binding in the brain by about 20 min in all groups. The highest correlation of BP_{ND}, calculated for the entire 90-min recording, and static SUVR ($R = 0.98$, $P < 0.0001$) was found for the time frame of 30–60 min after injection (Fig. 3), revealing this time [**Fig. 3**] window to be best suitable for further static analyses. Furthermore,

RGB

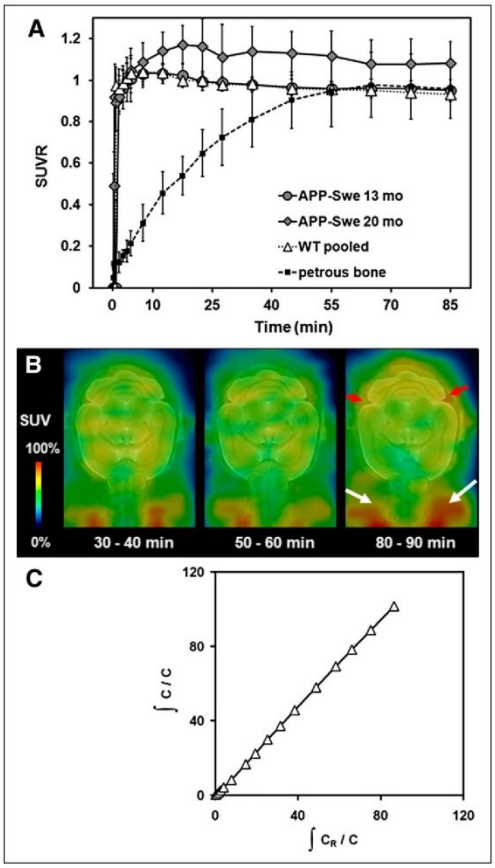

FIGURE 2. (A) Cortex-to-cerebellum ratios and petrous bone-to-cerebellum ratio as functions of time after ^{18}F-florbetaben administration in 13- and 20-mo-old transgenic APP-Swe mice and pooled WT mice (10–20 mo). Error bars indicate SD for estimates in groups of 5–10 transgenic and all WT animals. (B) Representative PET recording from various time frames of transgenic 16-mo old animal. Red arrows indicate progressive extracerebral activity in petrous bone, compared with earlier time frames, and white arrows indicate increased signal in frontal cranium and Harderian glands. (C) Corresponding Logan plot of frontal VOI in aged (20 mo) transgenic APP-Swe mice.

activity in petrous bone reached the cerebellar level at times after 60 min.

No significant age-dependent changes in ligand binding could be observed in the pilot study or likewise in the WT animals from the transgenic study. VOI-based analyses of the main study revealed significant SUVR differences, compared with baseline estimates (13 mo), in transgenic animals at the age of 16 mo (+7.9%; $P < 0.01$) [Fig. 4] and an increase by 16.6% at the age of 20 mo ($P < 0.001$) (Fig. 4A; Table 1).

Results for individual transgenic mice showed a continuous increase in tracer binding, whereas binding in WT animals remained constant over time (Figs. 4B and 4C). Figure 5 shows 2 representative coronal planes through the ventral frontal cortex of mean Logan BP_{ND} maps and SUVR maps in both WT and transgenic animals, revealing the increasing cortical uptake with age in transgenic mice. [Fig. 5]

Correlation with Histochemistry

Histochemical analyses revealed fibrillar β-amyloid plaques predominantly in the frontal cortex, complete absence in the cerebellum, and only a small amount in the hippocampus in some animals. In the 2 mice examined at the age of 13 mo, the plaque loads were 0.64% and 0.06%. In all transgenic mice surviving to 20 mo, the mean plaque load was 4.1% ± 2.8% (range, 1.0%–9.2%) in the frontal cortex VOI.

The correlation between percentage plaque load from histochemical analyses and SUVRs from PET recordings in similar volumes for the entire study group is depicted in Figure 6; PET [Fig. 6] results correlate highly significantly with the histochemical quantitation of plaque deposits ($R = 0.95$, $P < 0.001$). Autoradiographic findings ex vivo in representative young and aged transgenic animals are illustrated in Figure 6, and respective quantitation is presented in Table 1. The punctate distribution of β-amyloid labeling in the aged transgenic mouse, compared with findings in the young mouse, notably in the frontal cortex, concurs closely with histochemical findings and matches the anatomic location of increased tracer binding seen in the PET images.

Voxelwise Analyses

Voxelwise group contrasts between transgenic and WT animals are shown in Figure 7. By this exploratory approach, we were able [Fig. 7] to discern significant differences in ^{18}F-florbetaben uptake between transgenic and WT animals for the first time at 13 mo of age in a small cluster in the right frontal cortex. The spatial extent of this cluster progressed frontally and also parietally with increasing age, comprising 22,935 voxels at the age of 13 mo, 142,378 voxels at the age of 16 mo, and finally 278,692 voxels at the age of 20 mo (voxel size, 0.06 × 0.06 × 0.06 mm). No significant difference was observed subcortically, and white matter labeling remained constant over time. Similar results with identical patterns

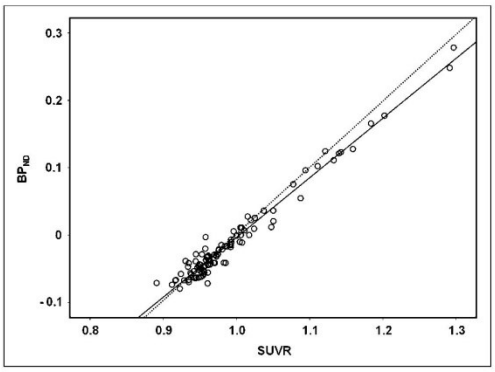

FIGURE 3. Correlation of ^{18}F-florbetaben BP_{ND} estimated from 90-min dynamic PET recordings with SUVR (cortex/cerebellum) results from 30- to 60-min static frame, estimated from cortical VOI in all mice. Dotted line represents perfect line of identity (BP_{ND} = SUVR − 1).

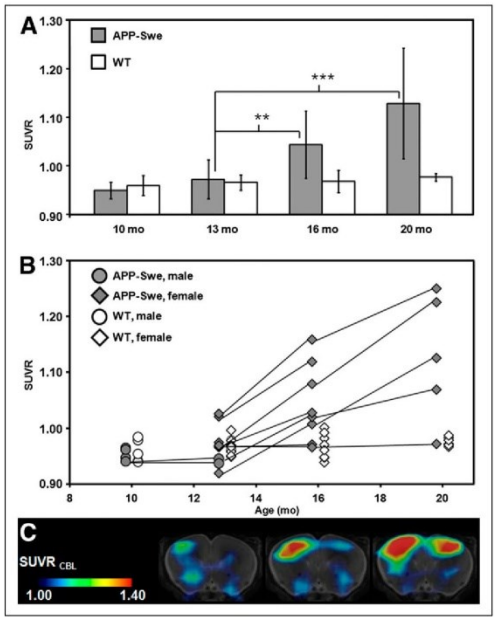

RGB

FIGURE 4. (A) VOI-based ^{18}F-florbetaben SUVR (cortex/cerebellum) group comparisons for transgenic APP-Swe mice (gray bar) and WT animals (white bar) aged 10, 13, 16, and 20 mo (mean ± SD). $^{**}P < 0.01$. $^{***}P < 0.001$ (2-sample t test). (B) Longitudinal intraindividual follow-up for all mice including pilot and main study animals. Black lines link consecutive data points for single transgenic animals (gray), whereas WT mice are depicted in white. Circles indicate male mice while diamonds display female mice. (C) Representative example for increasing signal over time for single transgenic mouse at the age of 13, 16, and 20 mo (left to right). Coronal planes show SUVR maps through ventral frontal cortex projected on MR imaging mouse atlas (gray scale). Asymmetry (right > left) with 11.4% at 20 mo of age was observed by small-animal PET and confirmed by histochemical analysis in this animal.

were obtained when contrasted against baseline scans of the transgenic animals. Voxelwise analyses of WT animals did not show any significant change in cortical or subcortical binding over time (data not shown).

Asymmetry

As an incidental finding arising from our approach of analyzing hemispheres separately, we noted some asymmetry of β-amyloid deposition in this mouse model. At the age of 20 mo, 2 animals showed a laterality index ((L − R)/(L + R)) (*22*) of greater than −0.04 in the PET scan (Fig. 4C), which was confirmed in the histochemical analyses and also the SPM voxelwise analysis—that is, greater ^{18}F-florbetaben uptake on the right side for the whole group (Fig. 7). This asymmetry tended to progressively develop with age in these mice.

VOI-Based and Histochemical Analyses in Hippocampus

There were no significant group differences for the hippocampal SUVR in the VOI-based analyses in mice at 20 mo of age, compared with baseline estimates (1.06 ± 0.10 vs. 1.02 ± 0.05; p = not significant); histochemical analysis revealed only very few plaques in this area for the group as a whole. In 1 of 7 transgenic mice, there were obviously more hippocampal plaques at the age of 20 mo (1.8%, compared with <1%), which concurred with the individual PET findings of higher SUVR than the mean of the whole transgenic group (1.22 vs. 1.06 ± 0.10).

DISCUSSION

We have performed the first, to our knowledge, longitudinal PET study in an AD mouse model using the novel amyloid tracer ^{18}F-florbetaben. Small-animal PET imaging for the sensitive monitoring of differences between transgenic and WT animals remains a challenge, due especially to the limited spatial resolution relative to the scale of target structures—that is, partial-volume effects—and, in the case of ^{18}F-labeled radiotracers such as ^{18}F-florbetaben, progressively increasing spillover of radioactivity from skull to brain. Despite these potential limitations, our PET procedure for quantitation of β-amyloid burden proved to be robust, yielding results that concur closely with histochemical findings and ex vivo autoradiography. We find that SUVR estimates derived from static recordings in the interval of 30–60 min after tracer injection give an excellent correlation with steady-state estimates of BP_{ND} from 90-min recordings; this approach with truncated acquisitions should reduce the loss of transgenic animals and facilitate scanning of larger groups in planned intervention studies.

The applicability of small-animal PET for monitoring β-amyloid accumulation has been a matter of some controversy. In 1 study with the bivalent radioligand 2-(1-{6-[(2-^{18}F-fluoroethyl)(methyl)amino]-2-naphthyl}ethylidene)malononitrile (^{18}F-FDDNP), which has high affinity for β-amyloid and also neurofibrillary tangles, there was no measurable increase in cerebral binding in 13- to 15-mo-old Tg2576 mice (*23*). This negative result led the authors to conclude that factors related to spatial resolution might fundamentally limit the suitability of molecular imaging for translational AD research in transgenic mice. Indeed, longitudinal PET studies with ^{18}F-FDDNP in triple-transgenic rats show increased binding in the frontal cortex and hippocampus, first evident at the age of 12 mo (*24*). This discrepancy may well reflect the greater target size in rats and consequently lesser partial-volume effects. Although the

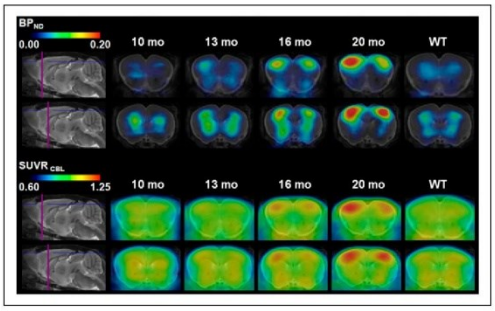

RGB

FIGURE 5. Coronal planes of mean ^{18}F-florbetaben BP_{ND} maps and corresponding mean SUVR maps through ventral frontal cortex at different ages of transgenic animals (10, 13, 16, and 20 mo) and pooled WT animals (10–20 mo; mean, 14.8 ± 3.4 mo) projected on MR imaging mouse atlas (gray scale).

RGB

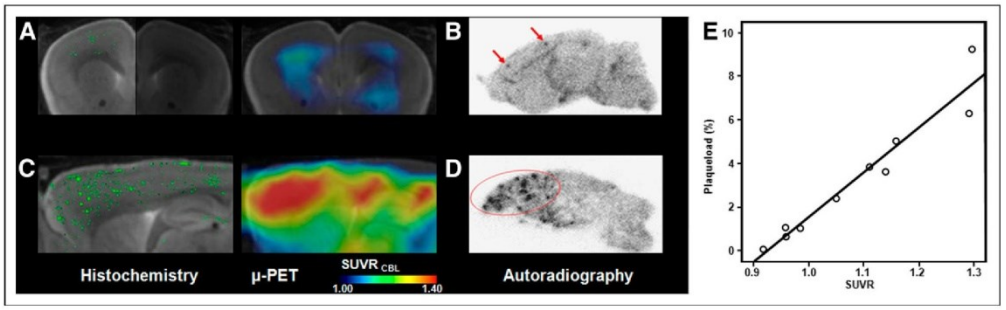

FIGURE 6. Multimodal imaging results for histochemical methoxy-X04 staining along with ^{18}F-florbetaben SUVR maps projected on MR imaging mouse atlas (gray scale) in vivo and corresponding images for autoradiography ex vivo. (A) Histochemistry in right hemisphere (bright side of image) and corresponding small-animal PET shown in coronal slice of 13-mo-old transgenic APP-Swe mouse. (B) Corresponding autoradiography in sagittal plane of left hemisphere in same animal. (C) Histochemistry in right hemisphere and corresponding small-animal PET shown in sagittal slice of 20-mo-old transgenic APP-Swe mouse. (D) Corresponding autoradiography in sagittal plane of left hemisphere in same animal. (E) Correlation of percentage plaque load as determined from histochemistry with SUVR analyses of ^{18}F-florbetaben PET in group of APP-Swe mice aged 13–20 mo. μ-PET = small-animal PET.

comparison of small-animal PET studies are difficult because of the use of different animal models, radiotracers, and study designs, our finding of progressive labeling of β-amyloid with ^{18}F-florbetaben in the cerebral cortex of APP-Swe mice stands in contrast to the earlier ^{18}F-FDDNP study in Tg2576 mice. Our results are also in contrast to those of a study with ^{11}C-Pittsburgh compound B (^{11}C-PIB) in aged Tg2576 mice, which had lower cortical binding than did WT mice. That paradoxical finding was attributed to confounding effects of cerebral blood flow and the low abundance of ^{11}C-PIB binding sites per plaque as expressed in mouse brain (*10*). However, a subsequent study with ^{11}C-PIB of high specific activity (>200 GBq/μmol) showed considerably more uptake in the cerebral cortex of aged APP23 mice than was seen in age-matched healthy controls (*7*). In that same study, there was an excellent correlation between PET results in the neocortex and those in the archicortex (i.e., hippocampus) and local β-amyloid burden (percentage) measured by histology—as likewise seen in the present ^{18}F-florbetaben study for the neocortex—but not in the hippocampus, in which specific signal was discernible only in 1 of 5 most aged APP-Swe mice. Thus, the factors accounting for the regional pattern of β-amyloid deposition in different transgenic mouse strains remain to be established. However, our findings generally concur with a recent multimodal validation of ^{11}C-PIB for PET studies of APP/PS1 mice, which showed excellent correlations between PET findings and the measurements of plaque burden obtained ex vivo and in vitro in the same animals (*8*), as likewise seen with another high-affinity ^{11}C-ligand based on the imidazo[2,1-b]benzothiazole scaffold (*25*). The manner in which different β-amyloid isoform patterns and the degree of fibrillarity contribute to PET imaging results remains to be elucidated. In a previous study in which the total amount of β-amyloid and its isoforms were considered (*8*), there was a highly significant correlation of total $A\beta_{40}$ and $A\beta_{42}$ quantification as assessed by enzyme-linked immunosorbent assay and histochemical findings (Thioflavin S staining) in forebrain structures. Notwithstanding, ^{18}F-florbetaben preferably binds to fibrillary plaques rather than diffuse amyloid (*14*), which is in concordance with the binding characteristics of the methoxy-X04 staining (*26*) performed in our study.

The authors of positive β-amyloid PET studies in transgenic mice have generally emphasized the importance of accurate, quality-controlled manual coregistrations and optimal procedures for image reconstruction, especially in studies of longitudinal design. On the basis of present experience, we concur with this conclusion and note that PET/CT and PET/MR multimodal imaging should facilitate spatial normalization in future studies, but that normalization is by no means absolutely essential.

The physical half-life of ^{18}F, which is 109 min, presents a practical advantage in the design of PET studies with tracers such as ^{18}F-FDDNP and ^{18}F-florbetaben and is furthermore a decisive factor for research centers lacking an on-site cyclotron or radiochemistry facility. However, rodents are especially apt to defluorinate many ^{18}F-labeled

RGB

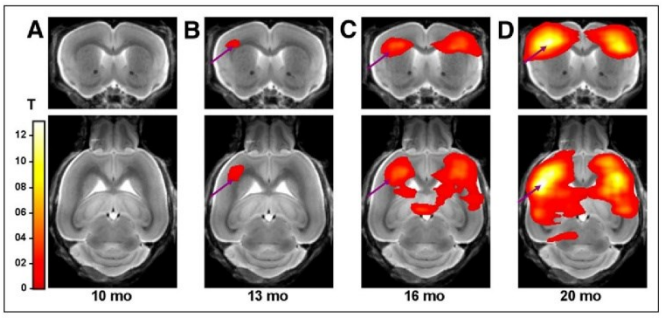

FIGURE 7. Longitudinal voxelwise group comparisons of ^{18}F-florbetaben SUVR maps in transgenic APP-Swe versus pooled WT animals (n = 27; age, 10–20 mo) with increasing age: 10 (A), 13 (B), 16 (C), and 20 (D) mo. 2-sample t test, $P < 0.001$, uncorrected for multiple comparisons, k > 20 voxel, projected on MR imaging mouse atlas (gray scale).

radiotracers, resulting in progressive labeling of the skeleton; spillover of radioactivity from the cranium to the brain can present a considerable obstacle to quantitation of brain PET, despite optimal image reconstruction with spatial resolution on the order of 1 mm. We have previously reported on the consequences of cranial labeling for quantitation of the cerebral binding of ^{18}F-labeled benzamides to dopamine receptors (*27,28*). In those studies, progressive contamination of the cerebellum reference tissue signal contributed importantly to a systematic underestimation of the magnitude of the ligand BP_{ND} in the striatum region of interest, despite an optimized iterative reconstruction procedure. Others have resorted to factor analysis for the correction of spill-in (*29*) or pharmacologic suppression of the pathway for radioligand defluorination (*30*). In the only previous rodent study using the ^{18}F-labeled amyloid tracer flutemetamol considering this issue (*9*), no significant defluorination was detected in rats in vivo, and the uptake in bone and brain were comparable at 120 min after injection. Similarly, we find that the magnitude of the cranial signal approaches that of the cerebellum reference tissue during ^{18}F-florbetaben recordings after 60 min (Figs. 2A and 2B). The time-dependent increase in net spillover to cerebral cortex propagates to declining SUVR and BP_{ND} estimates for circulation times after 60 min. However, we can substantially avoid this bias by selecting the time window of 30–60 min for ^{18}F-florbetaben quantitation and note that defluorination of this tracer occurs to a much lesser degree than in benzamide derivatives.

Unspecific white matter binding is a common feature of ^{18}F-labeled amyloid tracers (*31,32*) and to a lesser degree also of ^{11}C-PIB. The cerebral distributions of ^{18}F-flutemetamol and ^{11}C-PIB were compared in a recent PET and ex vivo and in vitro autoradiography study of Tg2576 mice and WT animals (*9*), revealing a slower clearance from white matter of the former compound, in line with its higher lipophilicity. We did not investigate plasma metabolites of the radiotracer in the present mouse study; as described earlier in humans (*33*), the preponderance of labeled metabolites was more hydrophilic than the parent compound, predicting poor penetration of metabolites into the brain. Retention of ^{18}F-florbetaben in the white matter of human brain exceeded that of ^{11}C-PIB (*32*). Because present PET methods cannot resolve cortical gray and white matter in mice, we measure in effect weighted mean radioactivity concentrations in the neocortex and in the cerebellum reference tissue. However, preferential binding in white matter can hardly be discerned, even by ex vivo autoradiography (Fig. 6). In any event, white matter contributions will tend to cancel out in SUVR and BP_{ND} calculations, a contention supported by the absolute lack of any spurious cortical signal in WT animals and young transgenic animals—that is, SUVR is 1 and BP_{ND} is 0, as likewise reported in earlier reports with ^{11}C-PIB (*8,34*). This lack of bias in baseline estimates of β-amyloid deposition allows us to estimate the sensitivity of our method for detecting β-amyloid to be approximately 1.5% plaque load (derived from Fig. 6E) in a defined area, relative to gold standard histology results.

Our voxelwise analysis detected a significant group difference in mice at the age of 13 mo, thus proving the suitability for the detection of mild neocortical amyloidogenesis in mice, as is well known in human PET studies of AD (*35,36*). In a recent study with the ^{18}F-florbetaben analog ^{18}F-florbetapir (*11*), increased binding in the cerebral cortex of APP/PS1 mice was already evident at 5 mo of age (+9% increase), but there was no evidence for a progressive increase by 12 mo. However, our longitudinal design revealed the spatial progression of cortical β-amyloid deposition in APP-Swe mice, and the present voxelwise statistical approach was particularly suited for revealing this amyloidogenesis (Fig. 7). This approach should serve in longitudinal intervention studies aimed at attenuating β-amyloid burden.

Whereas previous PET investigations in other AD models found symmetric labeling (*8*), a recent gene expression study has shown that transthyretin, a protein sequestering β-amyloid, was asymmetrically expressed in the adult brain of Tg2576 mice (*37*). We detected the first evidence of β-amyloid deposition on the right side of APP-Swe mice aged 13 mo, and this asymmetry, although small in magnitude, tended to remain in the subsequent PET investigations. Further investigation in larger groups would be required to determine whether this was a false-positive finding.

It was argued in a previous study using ^{18}F-florbetapir that the spatial resolution of current PET may simply be inadequate to detect β-amyloid in structures as small as the mouse hippocampus (*11*), although we note that it is the source intensity rather than spatial extent that ultimately determines the sensitivity of PET. We found the extent of hippocampal amyloidogenesis in APP-Swe mice to be vanishingly low in most mice, as proven by histochemistry. As the only mouse developing manifest β-amyloid plaques in the hippocampus showed higher plaque load in cortical areas as well, this finding was probably related to the overall penetrance of the trait. Hippocampal β-amyloid was reliably detected in a ^{11}C-PIB study of APP23 mice aged 20 mo (*7*); at present, it is uncertain if this reflects inherently greater sensitivity of the tracer or more likely the inherently greater penetrance of β-amyloid accumulation in the particular disease model.

We encountered a relatively high interanimal variability in percentage plaque burden in the transgenic animals, as confirmed by histochemical analyses. Not all animals could be followed to 20 mo; a transgenic model with faster plaque accumulation (such as double- or triple-transgenics) might present advantages arising from better anesthesia tolerance and general health in younger mice. However, because of our finding of adequate quantitation by shorter acquisition times, drop-out rates should decline in future longitudinal studies. Autoradiography was available only in a subset of animals and not in conjunction with histochemistry for the same hemisphere. Specific signal in the hippocampus of APP-Swe mice was too low for the reliable detection of β-amyloid by ^{18}F-florbetaben PET. Total amounts of soluble and insoluble β-amyloid species in mouse brain tissues as assessed by sandwich enzyme-linked immunosorbent assay were not performed, but in any event, we emphasize the fibrillary component for cross-validation of the PET signal.

CONCLUSION

In the most extensive longitudinal PET study yet conducted in an AD mouse model using an ^{18}F-labeled amyloid tracer, we demonstrated the first appearance of discernible β-amyloid plaque load at 13 mo and a progression to 20 mo. The magnitude of BP_{ND} calculated relative to the cerebellum was assessed by 90-min dynamic PET recordings but correlated precisely with SUVR measurements from static imaging at 30–60 min after injection. Furthermore, PET results with ^{18}F-florbetaben correlated closely with gold-standard histochemical analyses. SPM analysis of ^{18}F-florbetaben binding promises to serve admirably for monitoring the effects of interventions in longitudinal studies of APP-Swe mice.

DISCLOSURE

The costs of publication of this article were defrayed in part by the payment of page charges. Therefore, and solely to indicate this fact, this article is hereby marked "advertisement" in accordance with 18 USC section 1734. The study was sponsored by grants from SFB 596. No other potential conflict of interest relevant to this article was reported.

ACKNOWLEDGMENTS

Florbetaben precursor was kindly provided by Bayer Pharma AG. APP-Swe mice were generously provided by F. Hoffmann-La Roche AG. We thank Heidrun Zankl and Rosel Oos for excellent technical assistance.

REFERENCES

1. Ziegler-Graham K, Brookmeyer R, Johnson E, Arrighi HM. Worldwide variation in the doubling time of Alzheimer's disease incidence rates. *Alzheimers Dement.* 2008;4:316–323.
2. Weiner MW, Veitch DP, Aisen PS, et al. The Alzheimer's Disease Neuroimaging Initiative: a review of papers published since its inception. *Alzheimers Dement.* 2012;8:S1–S68.
3. Duyckaerts C, Delatour B, Potier MC. Classification and basic pathology of Alzheimer disease. *Acta Neuropathol.* 2009;118:5–36.
4. Hall AM, Roberson ED. Mouse models of Alzheimer's disease. *Brain Res Bull.* 2012;88:3–12.
5. Teipel SJ, Buchert R, Thome J, Hampel H, Pahnke J. Development of Alzheimer-disease neuroimaging-biomarkers using mouse models with amyloid-precursor protein-transgene expression. *Prog Neurobiol.* 2011;95:547–556.
6. Jucker M. The benefits and limitations of animal models for translational research in neurodegenerative diseases. *Nat Med.* 2010;16:1210–1214.
7. Maeda J, Ji B, Irie T, et al. Longitudinal, quantitative assessment of amyloid, neuroinflammation, and anti-amyloid treatment in a living mouse model of Alzheimer's disease enabled by positron emission tomography. *J Neurosci.* 2007;27:10957–10968.
8. Manook A, Yousefi BH, Willuweit A, et al. Small-animal PET imaging of amyloid-beta plaques with [^{11}C]PiB and its multi-modal validation in an APP/PS1 mouse model of Alzheimer's disease. *PLoS ONE.* 2012;7:e31310.
9. Snellman A, Rokka J, Lopez-Picon FR, et al. Pharmacokinetics of [^{18}F]flutemetamol in wild-type rodents and its binding to beta amyloid deposits in a mouse model of Alzheimer's disease. *Eur J Nucl Med Mol Imaging.* 2012;39:1784–1795.
10. Toyama H, Ye D, Ichise M, et al. PET imaging of brain with the beta-amyloid probe, [^{11}C]6-OH-BTA-1, in a transgenic mouse model of Alzheimer's disease. *Eur J Nucl Med Mol Imaging.* 2005;32:593–600.
11. Poisnel G, Dhilly M, Moustie O, et al. PET imaging with [^{18}F]AV-45 in an APP/PS1-21 murine model of amyloid plaque deposition. *Neurobiol Aging.* 2012;33:2561–2571.
12. Zhang W, Oya S, Kung MP, Hou C, Maier DL, Kung HF. F-18 polyethyleneglycol stilbenes as PET imaging agents targeting Abeta aggregates in the brain. *Nucl Med Biol.* 2005;32:799–809.
13. Zhang W, Oya S, Kung MP, Hou C, Maier DL, Kung HF. F-18 stilbenes as PET imaging agents for detecting beta-amyloid plaques in the brain. *J Med Chem.* 2005;48:5980–5988.
14. Fodero-Tavoletti MT, Brockschnieder D, Villemagne VL, et al. In vitro characterization of [^{18}F]-florbetaben, an Abeta imaging radiotracer. *Nucl Med Biol.* 2012;39:1042–1048.
15. Barthel H, Gertz HJ, Dresel S, et al. Cerebral amyloid-beta PET with florbetaben (^{18}F) in patients with Alzheimer's disease and healthy controls: a multicentre phase 2 diagnostic study. *Lancet Neurol.* 2011;10:424–435.
16. Richards JG, Higgins GA, Ouagazzal AM, et al. PS2APP transgenic mice, coexpressing hPS2mut and hAPPswe, show age-related cognitive deficits associated with discrete brain amyloid deposition and inflammation. *J Neurosci.* 2003;23:8989–9003.
17. Rominger A, Mille E, Zhang S, et al. Validation of the octamouse for simultaneous ^{18}F-fallypride small-animal PET recordings from 8 mice. *J Nucl Med.* 2010;51:1576–1583.
18. Dorr A, Sled JG, Kabani N. Three-dimensional cerebral vasculature of the CBA mouse brain: a magnetic resonance imaging and micro computed tomography study. *Neuroimage.* 2007;35:1409–1423.
19. Constantinescu CC, Mukherjee J. Performance evaluation of an Inveon PET preclinical scanner. *Phys Med Biol.* 2009;54:2885–2899.
20. Logan J, Fowler JS, Volkow ND, Wang GJ, Ding YS, Alexoff DL. Distribution volume ratios without blood sampling from graphical analysis of PET data. *J Cereb Blood Flow Metab.* 1996;16:834–840.
21. Sawiak SJ, Wood NI, Williams GB, Morton AJ, Carpenter TA. Voxel-based morphometry in the R6/2 transgenic mouse reveals differences between genotypes not seen with manual 2D morphometry. *Neurobiol Dis.* 2009;33:20–27.
22. Vernaleken I, Weibrich C, Siessmeier T, et al. Asymmetry in dopamine D(2/3) receptors of caudate nucleus is lost with age. *Neuroimage.* 2007;34:870–878.
23. Kuntner C, Kesner AL, Bauer M, et al. Limitations of small animal PET imaging with [^{18}F]FDDNP and FDG for quantitative studies in a transgenic mouse model of Alzheimer's disease. *Mol Imaging Biol.* 2009;11:236–240.
24. Teng E, Kepe V, Frautschy SA, et al. [F-18]FDDNP microPET imaging correlates with brain Abeta burden in a transgenic rat model of Alzheimer disease: effects of aging, in vivo blockade, and anti-Abeta antibody treatment. *Neurobiol Dis.* 2011;43:565–575.
25. Yousefi BH, Manook A, Drzezga A, et al. Synthesis and evaluation of ^{11}C-labeled imidazo[2,1-b]benzothiazoles (IBTs) as PET tracers for imaging beta-amyloid plaques in Alzheimer's disease. *J Med Chem.* 2011;54:949–956.
26. Klunk WE, Bacskai BJ, Mathis CA, et al. Imaging Abeta plaques in living transgenic mice with multiphoton microscopy and methoxy-X04, a systemically administered Congo red derivative. *J Neuropathol Exp Neurol.* 2002;61:797–805.
27. Rominger A, Wagner E, Mille E, et al. Endogenous competition against binding of [^{18}F]DMFP and [^{18}F]fallypride to dopamine $D_{2/3}$ receptors in brain of living mouse. *Synapse.* 2010;64:313–322.
28. Mille E, Cumming P, Rominger A, et al. Compensation for cranial spill-in into the cerebellum improves quantitation of striatal dopamine $D_{2/3}$ receptors in rats with prolonged [^{18}F]-DMFP infusions. *Synapse.* 2012;66:705–713.
29. Millet P, Moulin-Sallanon M, Tournier BB, et al. Quantification of dopamine $D_{2/3}$ receptors in rat brain using factor analysis corrected [^{18}F]fallypride images. *Neuroimage.* 2012;62:1455–1468.
30. Choi SR, Schneider JA, Bennett DA, et al. Correlation of amyloid PET ligand florbetapir F 18 binding with Abeta aggregation and neuritic plaque deposition in postmortem brain tissue. *Alzheimer Dis Assoc Disord.* 2012;26:8–16.
31. Herholz K, Ebmeier K. Clinical amyloid imaging in Alzheimer's disease. *Lancet Neurol.* 2011;10:667–670.
32. Rowe CC, Villemagne VL. Brain amyloid imaging. *J Nucl Med.* 2011;52:1733–1740.
33. Patt M, Schildan A, Barthel H, et al. Metabolite analysis of [^{18}F]Florbetaben (BAY 94-9172) in human subjects: a substudy within a proof of mechanism clinical trial. *J Radioanal Nucl Chem.* 2010;284:557–562.
34. Maeda J, Zhang MR, Okauchi T, et al. In vivo positron emission tomographic imaging of glial responses to amyloid-beta and tau pathologies in mouse models of Alzheimer's disease and related disorders. *J Neurosci.* 2011;31:4720–4730.
35. Barthel H, Luthardt J, Becker G, et al. Individualized quantification of brain beta-amyloid burden: results of a proof of mechanism phase 0 florbetaben PET trial in patients with Alzheimer's disease and healthy controls. *Eur J Nucl Med Mol Imaging.* 2011;38:1702–1714.
36. Förster S, Grimmer T, Miederer I, et al. Regional expansion of hypometabolism in Alzheimer's disease follows amyloid deposition with temporal delay. *Biol Psychiatry.* 2012;71:792–797.
37. Tsai KJ, Yang CH, Lee PC, Wang WT, Chiu MJ, Shen CK. Asymmetric expression patterns of brain transthyretin in normal mice and a transgenic mouse model of Alzheimer's disease. *Neuroscience.* 2009;159:638–646.

NeuroImage 84 (2014) 843–853

Contents lists available at ScienceDirect

NeuroImage

journal homepage: www.elsevier.com/locate/ynimg

Impact of partial volume effect correction on cerebral β-amyloid imaging in APP-Swe mice using [^{18}F]-florbetaben PET☆

Matthias Brendel [a], Andreas Delker [a], Christina Rötzer [a], Guido Böning [a], Janette Carlsen [a], Clemens Cyran [b], Erik Mille [a], Franz Josef Gildehaus [a], Paul Cumming [c], Karlheinz Baumann [d], Harald Steiner [f,g], Christian Haass [e,f,g], Jochen Herms [e,f,h], Peter Bartenstein [a,e], Axel Rominger [a,*]

[a] Department of Nuclear Medicine, Ludwig-Maximilians-University, Munich, Germany
[b] Department of Clinical Radiology, Ludwig-Maximilians-University, Munich, Germany
[c] Department of Nuclear Medicine, University of Erlangen/Nuremberg, Germany
[d] F. Hoffmann-La Roche, Basel, Switzerland
[e] Munich Cluster for Systems Neurology (SyNergy), Munich, Germany
[f] German Center for Neurodegenerative Diseases (DZNE), Ludwig-Maximilians-University, Munich, Germany
[g] Adolf-Butenandt-Institute, Biochemistry, Ludwig-Maximilians-University, Munich, Germany
[h] German Center for Neurodegenerative Diseases (DZNE) - Department for Translational Brain Research, Ludwig-Maximilians-University, Munich, Germany

ARTICLE INFO

Article history:
Accepted 10 September 2013
Available online 20 September 2013

Keywords:
Partial volume effect correction
Small animal PET
Alzheimer's disease
ß-amyloid
[^{18}F]-florbetaben

ABSTRACT

We previously investigated the progression of β-amyloid deposition in brain of mice over-expressing amyloid-precursor protein (APP-Swe), a model of Alzheimer's disease (AD), in a longitudinal PET study with the novel β-amyloid tracer [^{18}F]-florbetaben. There were certain discrepancies between PET and autoradiographic findings, which seemed to arise from partial volume effects (PVE). Since this phenomenon can lead to bias, most especially in the quantitation of brain microPET studies of mice, we aimed in the present study to investigate the magnitude of PVE on [^{18}F]-florbetaben quantitation in murine brain, and to establish and validate a useful correction method (PVEC).
Phantom studies with solutions of known radioactivity concentration were performed to measure the full-width-at-half-maximum (FWHM) resolution of the Siemens Inveon DPET and to validate a volume-of-interest (VOI)-based PVEC algorithm. Several VOI-brain-masks were applied to perform in vivo PVEC on [^{18}F]-florbetaben data from C57BL/6(N = 6) mice, while uncorrected and PVE-corrected data were cross-validated with gamma counting and autoradiography. Next, PVEC was performed on longitudinal PET data set consisting of 43 PET scans in APP-Swe (13–20 months) and age-matched wild-type (WT) mice using the previously defined masks. VOI-based cortex-to-cerebellum ratios (SUVR) were compared for uncorrected and PVE-corrected results. Brains from a subset of transgenic mice were ultimately examined by autoradiography ex vivo and histochemistry in vitro as gold standard assessments, and compared to VOI-based PET results.
The phantom study indicated a FWHM of 1.72 mm. Applying a VOI-brain-mask including extracerebral regions gave robust PVEC, with increased precision of the SUVR results. Cortical SUVR increased with age in APP-Swe mice compared to baseline measurements (16 months: +5.5%, $p < 0.005$; 20 months: +15.5%, $p < 0.05$) with uncorrected data, and to a substantially greater extent with PVEC (16 months: +12.2% $p < 0.005$; 20 months: +36.4% $p < 0.05$). WT animals showed no binding changes, irrespective of PVEC. Relative to autoradiographic results, the error [%] for uncorrected cortical SUVR was 18.9% for native PET data, and declined to 4.8% upon PVEC, in high correlation with histochemistry results. We calculate that PVEC increases by 10% statistical power for detecting altered [^{18}F]-florbetaben uptake in aging APP-Swe mice in planned studies of disease modifying treatments on amyloidogenesis.

Abbreviations: APP-Swe, K670N; M671L, mutation of amyloid precursor protein; BAS, basal surround VOI; BGR, background surround VOI; CBL, cerebellum; CTX, cortex; ET, effects of therapy; FoV, Field of View; FWHM, full width at half maximum; FRO, frontal surround VOI; GTM, geometric transfer matrix; HGL, harderian gland VOI; HIP, hippocampus; PVE, partial volume effects; MGM, Müller-Gärtner Method; MIX, combined brain structure VOI except frontal cortical target VOI and cerebellum; MIX-HI, high uptake part of subdivided MIX VOI; MIX-LO, low uptake part of subdivided MIX VOI; PSF, point spread function; PVEC, partial volume effect correction; RMSE [%], root–mean–square-error percentage; SPI, spinal surround VOI; SRR, single extracerebral surround VOI; SUP, superior surround VOI; TG, transgenic; WT, wild-type.

☆ Financial support: The study was supported by the SyNergy Cluster.
* Corresponding author. Fax: +49 89 7095 7646.
E-mail address: axel.rominger@med.uni-muenchen.de (A. Rominger).

1053-8119/$ – see front matter © 2013 Elsevier Inc. All rights reserved.
http://dx.doi.org/10.1016/j.neuroimage.2013.09.017

Introduction

Alzheimer's disease (AD) is imposing a growing socioeconomic burden due to the aging population demographics, especially in industrialized nations (Ziegler-Graham et al., 2008). Present treatments are symptomatic, but some promising avenues for disease-modifying treatment are in different phases of development and approval (Singh et al., 2012). In general animal models represent an important tool for preclinical testing of disease progression and novel medications in conjunction with molecular imaging (Virdee et al., 2012). A number of rodent AD-models are characterized by cerebral overexpression of ß-amyloid and progressive formation of cortical ß-plaques, emulating this aspect of AD pathology (Teipel et al., 2011). The prospect of monitoring disease progression in individual animals has given rise to a number of rodent positron emission tomography (PET) studies in conjunction with [^{11}C]- or [^{18}F]-labeled ß-amyloid-tracers (Klunk et al., 2005; Maeda et al., 2007; Manook et al., 2012; Poisnel et al., 2012; Rojas et al., 2013; Snellman et al., 2012; Toyama et al., 2005). Quantitative analysis of PET data from rodent brain is necessarily compromised by partial volume effects (PVE), which result in degradation of signals from target sources of the same scale as the spatial resolution of the tomograph (Kuntner et al., 2009). However, there have been few reports of small animal PET–PVE, despite its great significance for PET quantification (Erlandsson et al., 2012). In the majority of previous human studies, PVE correction (PVEC) of brain signals has been based on the Müller–Gärtner Method (MGM) and its modifications (Thomas et al., 2011) which depend on voxel-based geometric transfer matrix (GTM) models first established by Videen and coworkers (Videen et al., 1988).

We previously investigated the progression of β-amyloid deposition in brain of AD-model mice over-expressing a human mutation of the amyloid-precursor protein (APP-Swe), in a longitudinal PET study with the novel β-amyloid tracer [^{18}F]-florbetaben (Rominger et al., 2013). We reported a notable increase in β-amyloid PET signal from the brain of APP-Swe mice with age, which significantly correlated with histochemical findings post mortem. However, there were also distinct discrepancies between cortex-to-cerebellum standard uptake value ratios (SUVR) measured by PET in vivo and the more pronounced accumulation measured ex vivo. Similar discrepancies have been described in a study with the alternate β-amyloid tracer [^{18}F]-AV-45 (Poisnel et al., 2012), and are likely attributable to PVE.

With this background, we aimed to establish the magnitude of PVE on quantitation of β-amyloid burden in the mouse brain with [^{18}F]-florbetaben, and to implement and validate PVEC for our AD mouse model. We predicted that PVE-correction of PET recordings should enhance the precision of the method, this affording more sensitive detection of planned disease-modifying treatments and to reductions in required sample sizes.

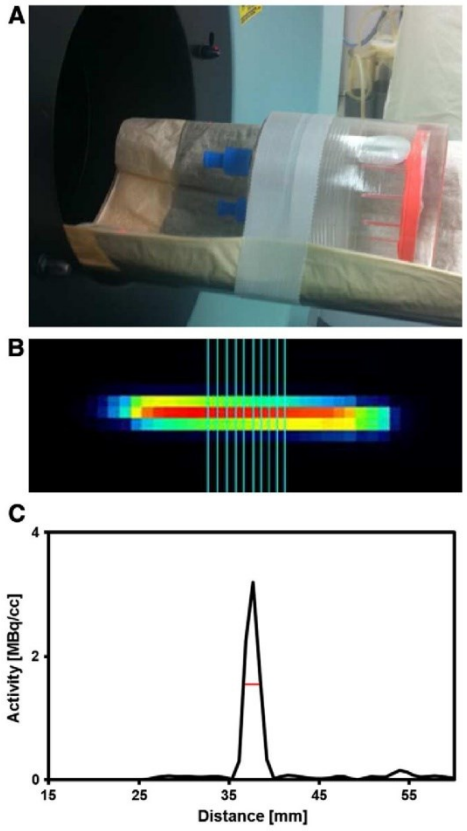

Fig. 1. (A) [^{18}F]-filled cylindric phantom in transaxial position in front of the aperture of the small animal PET scanner. Cannulae appear red due to filling with eosin marker solution and contain [^{18}F] at a range of radioactivity concentrations. They are fixed in transaxial position with modeling clay (orange) within the phantom. (B) Corresponding PET scan of a [^{18}F]-filled single cannula (inner diameter 0.8 mm) immersed in an [^{18}F]-background of 1000-fold less activity concentration. Voxel dimensions are 0.78 × 0.78 × 0.80 mm, i.e. oversampled relative to the FWHM. Blue lines in axial direction show applied line profiles. (C) Resulting line profile as a function of distance for averaged 120 line profiles in the horizontal axial direction. Red line indicates the mean FWHM value (1.72 mm) arising from this calculation.

Materials and methods

Phantom studies

Estimation of spatial resolution

Indwelling venous cannulae (Vasofix® Safety; B. Braun Melsungen AG, Germany) of three different internal diameters (0.4, 0.6 and 0.8 mm) were cut into 20 mm lengths, filled with a solution containing eosin and [^{18}F] (61.56 MBq/cc), and sealed at both ends with superglue. Two sources of each diameter were placed in a cylindrical phantom chamber (volume 41.2 ml), and held in place with modeling clay at an interval of 8 mm (Fig. 1A). The phantom chamber was then filled with water containing [^{18}F] (0.07 MBq/cc), i.e. background activity approximately 0.1% of the target activity concentration. The phantom was then placed in the aperture of the Siemens Inveon DPET, with the tubular sources in horizontal orientation. The acquisition protocol consisted of a 60 min emission scan, followed by a 15 min transmission scan using a rotating [^{57}Co] point source, resulting in a single frame (3600 s). A second acquisition was acquired after rotating the phantom by 90°, placing the tubular sources in a vertical orientation. As described in detail previously, (Rominger et al., 2013) the reconstruction consisted of 4 OSEM3D and 32 MAP3D iterations, a zoom of 1.0, with scatter and decay correction, resulting in a final 128 × 128 × 159 matrix of voxels measuring 0.78 × 0.78 × 0.80 mm. The reconstruction algorithm as implemented by the tomograph's manufacturer accounts for the space-variant detector response and yields a high and nearly space-invariant spatial resolution (Qi and Leahy, 2000; Visser et al., 2009). Due to the improved resolution properties of this algorithm it provides substantially enhanced quantitative accuracy compared to standard filtered back projection, even in case of low count statistics in dynamic PET measurements (Cheng et al., 2012).

Line profiles were generated within Amide image analyzing software (V0.8.22; http://amide.sourceforge.net) in ten consecutive voxel-layers through the midline of each cannula in the X and Y

planes, followed by calculation the mean (±SD) full-width-at-half-maximum (FWHM) of 40 measurements of the several cannula diameters (Fig. 1B). The procedure was repeated in Z-plane using the recording of the rotated phantom. Effects of cannula internal diameter were determined by a one-way analysis of variance (ANOVA) using SPSS (version 21.0; SPSS, Chicago, IL).

PVEC algorithm

All PVEC estimations were performed using a volume-of-interest (VOI) -based approach (Rousset et al., 1998) implemented in PMOD (V3.4, PMOD Technologies Ltd.) (Rousset et al., 2008). Requirements of this method consist of an invariant point spread function (PSF) within the system, accurate knowledge of the spatial resolution of the instrument and homogeneous tissue uptake within previously defined VOIs (Lehnert et al., 2012). Regional PSFs (RSF) are calculated through integration of single tissue domains' PSF, and used for computation of weighting factors representing the contributions of the set of tissue domains among each other. The RSF of a given VOI_i is therefore expressed in terms of r and r', which represent 3-dimensional vectors in the image space, and where $h(r,r')$ is the PSF of the PET scanner (Rousset et al., 2008):

$$\mathrm{RSF}_i(r) = \int_{VOI_i} h(r,r')dr' \tag{1}$$

The mathematical dependence of the true radioactivity T_i in a VOI_i and the observed radioactivity concentration t_j within a region ROI_j – where ω_{ij} represents the contribution of tissue component VOI_i to ROI_j as weighting factors – is given by:

$$t_j = \sum_{i=1}^{n} \omega_{ij} T_i \tag{2}$$

which can be expressed as:

$$\omega_{ij} = \frac{1}{v_j} \int_{ROI_j} \mathrm{RSF}_i(r)dr \tag{3}$$

where v_j is the total volume of ROI_j. A matrix of regional transfer coefficients is generated through the ω_{ij} factors, while calculation of PVE-corrected radioactivity concentrations in previously defined VOIs is performed through multiplication of original PET data by the inverted GTM. The PVE-corrected images contain only those regions with VOI-mask definitions.

Chessboard experiment

Evaluation of VOI-based PVE-correction with acquisition and reconstruction parameters as described above for structures of the scale of a mouse brain was accomplished by a second phantom study. Here, 40 adjacent square wells of a 96-well laboratory plate (12 × 8 wells; each well was 30 mm deep and of 8.06 mm cross section, separated by walls of 0.91 mm thickness), were filled with 1.5 ml each of solutions containing [^{18}F] at five different radioactivity concentrations (Fig. 2A). The range of concentrations was selected to match observations in recent [^{18}F]-florbetaben scans of mouse brain. The radioactivity concentrations were measured in a well-counter (Model VDC-404, Veenstra Instruments) cross-calibrated to the tomograph, and used as the gold standard for calculation of percentage root–mean–square-errors (RMSE [%]) in corresponding PET results according to:

$$\mathrm{RMSE}[\%] = 100 \times \frac{\sqrt{\sum_{i=1}^{n} (A_{meas} - A_{true})^2}}{\sqrt{\sum_{i=1}^{n} (A_{true})^2}} \tag{4}$$

Where n is the number of filled wells, A_{true} is the cross-calibrated activity and A_{meas} is the concentration recording in the PET scan.

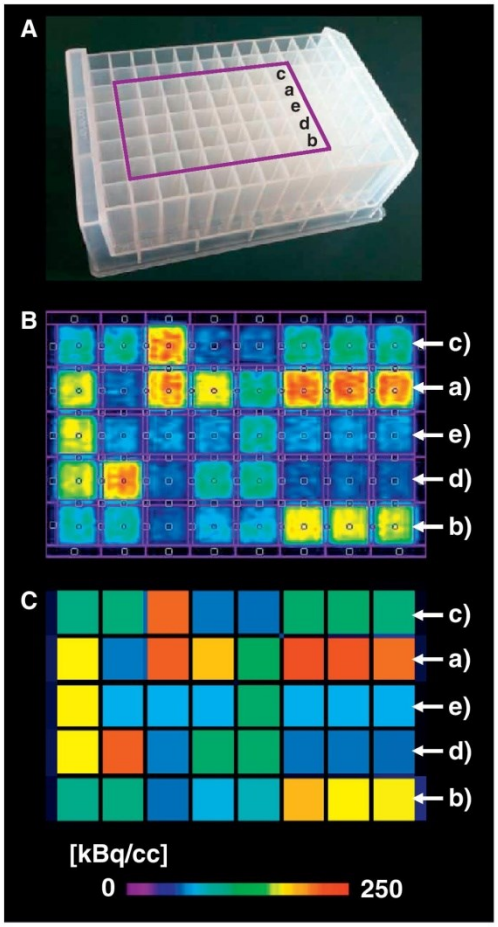

Fig. 2. (A) Polyethylene (PE-LD) 2000 µl deep-well plate with 96 wells. Edge length of wells is 8.06 mm and wall thickness is 0.91 mm. Purple rectangle shows an 8 × 5 well-field filled with cross-calibrated [^{18}F]-sources at five different activity concentrations. Sets of three equal filled wells on the right of each row represent concentrations of (a) 225.3,(b) 182.7,(c) 93.6,(d) 61.3, and (e) 41.5 kBq/cc. (B) VOI-mask containing 161 single regions (40 representing wells/121 representing borders or edges) applied to 60 min static PET recording. Absolute dimensions of the corrected field are 111.6 mm at 8-well side, 46.3 mm at 5-well side, and depth of 6.4 mm. (C) Corresponding PVE-corrected PET data (FWHM 1.72 mm).

The phantom was placed in the scanner with the 12-well side along the z-axis and the 8-well side along the x-axis, and emission recordings were acquired and reconstructed as described above. 161 cuboidal VOIs representing wells, borders and surrounding area of the plane defined by the 8 × 5 well-field plane (111.6 × 46.3 mm in total and a height of 6.4 mm) were defined as a template, using the PMOD fusion tool to co-register the PET (Fig. 2B) image to the transmission scan. The VOI-based PVEC algorithm using the appropriate FWHM was applied (Fig. 2C). RMSE [%] of the VOI-values for all cubes were compared for uncorrected and PVE-corrected data. Finally, the correction process was performed using FWHM estimates extending over ±5 SDs to study the influence of this parameter on signal recovery.

Animal studies

All experiments were performed in compliance with the National Guidelines for Animal Protection, Germany, and the approval of the animal care committee.

MRI template acquisition

Magnetic resonance imaging of the mouse brain was performed on a clinical 3 Tesla system (Magnetom Verio, Siemens Healthcare, Erlangen, Germany) with animals in headfirst prone position, using a dedicated small animal coil (RAPID MR International, Columbus, OH). The protocol consisted of a T2-weighted turbo spin echo, a T1-weighted 3D FLASH and a T1-weighted MPRAGE sequence. The parameters for Turbo Spin Echo were TR/TE = 7800/69; 20 slices; slice thickness 0.7 mm; 4 averages and total imaging time 10:01 min, for 3D FLASH TR/TE = 12.6/6.28; 36 slices per slab; slice thickness 0.5 mm; flip angle 30.0°; 4 averages and total imaging time 6:27 min. Both sequences were obtained using the same in-plane resolution with a field of view of 64 × 64 mm and a 256 × 256 matrix. The parameters for MPRAGE were TR/TE = 15/4.76; 20 slices per slab; slice thickness 0.8 mm; 1 average; field of view (FoV) 180 × 180 mm; 256 × 256 matrix and total imaging time 1:21 min. Sagittal contour VOIs were drawn in each slice of a sagittal T2-weighted sequence using PMOD and finally combined to a whole brain VOI-mask (Fig. 3A).

Point spread function simulation for a mouse brain

Single static frames lasting 30 min was acquired 30–60 min after intravenous application of 8.9 ± 2.7 MBq [^{18}F]-florbetaben to 22 C57BL/6 wild-type(WT) animals, were normalized to global mean activity and co-registered to the MRI as described previously (Rominger et al., 2013). Based upon our earlier 90 min dynamic emission recordings, we found the magnitude of $SUVR_{CTX/CBL}$ to be stable in this interval, and relatively unaffected by spill-in of cranial radioactivity signal (Rominger et al., 2013). A group average SUV-image (Fig. 3B) was calculated and the whole cerebral MRI mask was applied. Voxels outside the mask were set to zero intensity, while the brain mask image was blurred with a Gaussian filter to the FWHM assessed from the cannula phantom, so as to measure the probable magnitude of spillover as a function of distance from the mask edge. A threshold of >0.01% was set as the limit for extracerebral spillover, which defined the spatial extent of extracerebral VOIs defined in further analyses (Fig. 3C), aiming to achieve optimal consideration of both spilled-in and spilled-out activity, even of very bright sources.

VOI-mask definition

PVEC in the mouse brain was investigated by applying the VOI-based approach depending on the anatomical structures of 20 months old C57BL/6 animals as defined by 3 T structural MRI. As the assumption of homogenous tissue uptake within each defined compartment is a prerequisite of the Rousset method, we examined the effect of subdividing larger structures that showed signs of inhomogeneity in tracer uptake. Furthermore, VOI templates defining the Harderian glands and other extracerebral structures were included in the analysis. A visual overview of all defined regions is provided in Supplement 1, comprehensive specifications can be found in Table 1: Bilateral VOIs of frontal cortex (CTX) comprising 9 mm^3 each were defined as previously (Rominger et al., 2013), or a more extensive frontal cortex volume comprising a total of 30 mm^3 was used (CTX_{LARGE}). A cerebellar VOI (CBL) comprising 64 mm^3 was defined according to the mean of MRI from four representative mice. The remaining cerebrum was defined as a single VOI of volume 409 mm^3 (MIX), or further subdivided in two hippocampal VOIs (HIP) each comprising 6.5 mm^3, a higher uptake region (MIX-HI; 69 mm^3) and a lower uptake region (MIX-LO; 327 mm^3). MIX-HI mostly represents axonal fibers such as cerebellar peduncle, corticospinal tract or basal ganglia loops which typically show unspecific white matter uptake of [^{18}F]-florbetaben, as seen in humans (Villemagne et al., 2011). Therefore the uptake-classification was based on segmentation of the spatially averaged [^{18}F]-florbetaben data in

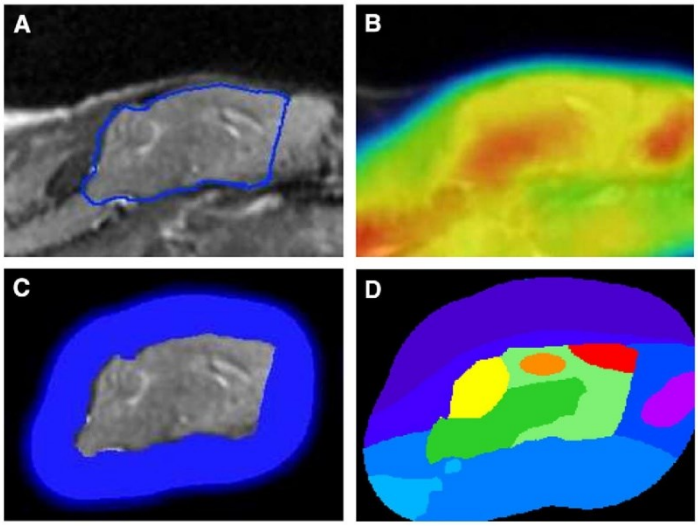

Fig. 3. (A) Representative sagittal MRI (T2-weighted) slice of a 20 month old female C57BL/6 animal. Blue line illustrates conture-VOIs as drawn on each single slice and finally combined to a whole brain mask. (B) Averaged [^{18}F]-florbetaben PET image (C57BL/6, N = 22) in corresponding sagittal slice. (C) Averaged [^{18}F]-florbetaben emission image (C57BL/6, N = 22) blurred with a filter of 1.72 mm after extracerebral masking using a whole brain MRI (overlay, center). Intensity threshold for included surrounding extracerebral regions (blue) was set at > 0.01‰ activity. (D) Subdivided VOI-mask containing seven cerebral and six extracerebral regions. Cerebral regions are defined in following colors: CTX = red, HIP = orange, CBL = yellow, MIX-HI = dark green, MIX-LO = light green. Extracerebral regions: Harderian glands = purple, other surrounding areas are depicted in blue shades.

Table 1
Sizes of VOIs and compositions of VOI-masks. Different sizes of CTX and MIX regions depend on usage of either small or large CTX VOI.

VOI	Size [mm^3]	4-Region			7-Region		
		None	1-EXT	6-EXT	None	1-EXT	6-EXT
Cerebral							
CTX (small/large)	19/30	x	x	x	x	x	x
CBL	64	x	x	x	x	x	x
MIX	398/409	x	x	x			
HIP	13				x	x	x
MIX-HI	69				x	x	x
MIX-LO	316/327				x	x	x
Extracerebral							
SRR	2702		x			x	
HGL	77			x			x
FRO	226			x			x
SPI	48			x			x
BAS	799			x			x
SUP	452			x			x
BGR	1100			x			x

(N = 22) C57BL/6 WT mice, which lack discernible subcortical differences, as compared to APP-Swe animals (Rominger et al., 2013), with intensity thresholds capturing the boundaries of these white matter regions.

Extracerebral regions were depicted either as a single surrounding VOI comprising $2.7 * 10^3$ mm^3 (SRR) or divided into six parts consisting of a Harderian gland VOI (HGL; 77 mm^3), a frontal VOI (FRO; 226 mm^3) encircling the Harderian glands, and extending to the brain frontal pole, a spinal VOI (SPI; 48 mm^3), a basal VOI (BAS; 799 mm^3), a superior VOI (SUP; 452 mm^3), and a background VOI posterior to the mouse head (BGR; $1.1 * 10^3$ mm^3). These classifications were based on conjunctive analysis of PET and MRI data.

In the evaluation of the PVEC algorithm, a four-region-model (2 × CTX, CBL and MIX) was combined with either none, one (SRR) or six extracerebral compartments (HGL, FRO, SPI, BAS, SUP and BGR). A seven brain region-model (2 × CTX, CBL, 2 × HIP, MIX-HI and MIX-LO) was contrasted with the four-region-model to study the influence of number of segments on stability of the PVEC. In addition, all masks were defined with CTX_{LARGE} VOIs instead of the original CTX VOIs, so as to examine effects arising from small diameter spans of the target VOI. Fig. 3D shows a mask containing all 13 VOIs.

VOI-mask validation

Six C57BL/6 WT female mice (25.2 ± 3.2 g; 10.1 ± 1.5 months of age) were anesthetized with 1.5% isoflurane and [^{18}F]-florbetaben (10.2 ± 0.7 MBq) was injected through a tail vein. Emission recordings consisting of a single frame (30–60 min p.i.) were followed by a 15 min transmission scan, and reconstruction algorithms were likewise as described above. Immediately upon conclusion of the PET sessions, mice were decapitated, the brains were removed and then sagittally bisected. The right hemisphere was frozen by immersion in isopentane (−40°C) and 20 μm thick sagittal slices were cut with a Leica CM 1510–1 Cryostat (Leica Microsystems, Nussloch Germany), and mounted on glass slides within 60 min post mortem. An imaging plate(Fujifilm; BAS cassette2 2025) was exposed to the slides for 10 h, scanned at 25 μm resolution with Raytest equipment (CR 35 BIO, Dürr Medical, Germany), and analyzed with AIDA image analyzing software (V4.50). Here, we drew the cerebellar and frontal cortical regions-of-interest (ROIs) analog to PET-VOIs, which were used for calculation of the cortex-to-cerebellum standard uptake value ratios ($SUVR_{CTX/CBL}$) ex vivo.

Left hemispheres were dissected into cerebellum, two frontal cortical regions (anterior and posterior) and the remaining brain. These tissues were weighed, and radioactivity concentrations were measured in a gamma counter (Cobra Quantum 5002, Packard) cross-calibrated to the tomography, with decay-correction to time of tracer injection for final SUV calculations.

PET data was reconstructed and co-registered to MRI as described above, and the several VOI-based PVECs were applied. A total of twelve different masks (Table 1) were analyzed and SUV of all regions as well as $SUVR_{CTX/CBL}$ were calculated both for uncorrected and PVE-corrected PET data. Left hemisphere frontal cortical and cerebellar PET-SUV of uncorrected and PVE-corrected data were compared with corresponding gold standard values measured by gamma counting as mean error [%] ± SD. For the right hemisphere, the calculation of $SUVR_{CTX/CBL}$ by PET and gold standard autoradiography results (considered as the true uptake ratio) were expressed as mean error [%] ± SD. For subsequent animal studies, the most valid VOI-mask was selected based on minimization of error [%] in PET $SUVR_{CTX/CBL}$ (versus autoradiography) and PET SUV (versus gamma counting).

Application to longitudinal [^{18}F]-florbetaben PET data

Animal and acquisition parameters. The VOI-based approach using the masks emerging from the validation process was applied to 21 PET scans longitudinally recorded from female transgenic mice (TG) overexpressing human APP with the Swedish double mutation (K670N, M671L) driven by the mouse Thy1.2 promoter (Richards et al., 2003). The TG group was subdivided into groups aged 13 (N = 8), 16 (N = 8) and 20 (N = 5) months. The group of 22 female C57BL/6 WT mice of age extending from 13 to 20 months were pooled, given the lack of age-dependent changes in [^{18}F]-florbetaben uptake (Rominger et al., 2013). As above, single frame emission recordings at 30–60 min after application of [^{18}F]-florbetaben (8.9 ± 2.7 MBq) i.v. were followed by a 15 min transmission scan. Reconstruction, normalization and co-registration of PET images was performed as described above.

Effects of PVEC on VOI-based data. Computation of PVE-corrected data was performed using the measured FWHM and the defined VOI-masking in PMOD. Uncorrected VOI measurements were calculated as percentage of the corresponding PVE-corrected VOI-values. The SUVR were calculated for CTX and HIP relative to CBL for uncorrected and PVE-corrected values. $SUVR_{CTX/CBL}$ of 16 and 20 month old TG animals were compared against the "baseline" measurements at age of 13 months.

Effects of PVEC on histological and autoradiography data. Correlations of PET $SUVR_{CTX/CBL}$ with histological analyses as assessed by Methoxy-X04 staining (Klunk et al., 2002) were calculated for ten hemispheres from 13 and 20 month old TG animals and contrasted between uncorrected and PVE-corrected $SUVR_{CTX/CBL}$ values. Details of histological image acquisition and analysis are presented elsewhere (Rominger et al., 2013). Furthermore, uncorrected and PVE-corrected PET $SUVR_{CTX/CBL}$ values from pairs of TG mice aged 13 and 20 months of age, and a pair of WT mice aged 20 months were compared with corresponding gold standard $SUVR_{CTX/CBL}$ derived from autoradiography ex vivo as error [%] ± SD.

Effects of PVEC on power calculations

The variance in individual Δ-$SUVR_{CTX/CBL}$-[%] measurements during the age interval of 13 to 16 months in our group of eight (untreated) TG animals has direct implications for the planning of future studies with an intervention arm, based upon a power calculation as follows: Relative to an untreated group (Δ-$SUVR_{CTX/CBL}$-$[\%]_{untreated}$), and assuming effect of therapy (ET) in the range 30–70%, expected Δ-$SUVR_{CTX/CBL}$-$[\%]_{treated}$ values and consequent power in a treatment-group were calculated by Eq. (5):

$$\Delta SUVR_{CTX/CBL}[\%]untreated = \Delta SUVR_{CTX/CBL}[\%]_{treated} \times (1-ET) \quad (5)$$

Using the program G * Power (V3.1.6; University of Kiel, Germany) we contrasted presumed independent means of Δ-$SUVR_{CTX/CBL}$-[%] for

treated and untreated groups of animals separately for uncorrected and PVE-corrected data.

Statistics

Group comparisons of correction [%] were assessed for each VOI by one-way ANOVA and Tukey post-hoc test for multiple comparisons. Follow-up group comparisons of VOI-based PET results measured as SUVR in TG mice were performed using a paired Student's *t*-test, calculated by IBM SPSS Statistics. For correlation analyses Pearson's coefficients of correlation (R) were calculated. A threshold of $p < 0.05$ was considered to be significant for rejection of the null hypothesis.

Results

Phantom studies

Estimation of spatial resolution

Mean FWHM was identical for all three internal diameters of [^{18}F]-filled cannula sizes ($F = 0.034$; p = n. s.), and indicated an isotropic spatial resolution of 1.72 ($\pm$0.08) mm (Fig. 1C).

Chessboard experiment

Cross-calibrated standard radioactivity concentrations were 225.3, 182.7, 93.6, 61.3, and 41.5 KBq/cc. Uncorrected data revealed RMSE [%] ranging from 14.2% to 24.3% (Fig. 4A), while corresponding PVE-corrected data showed RMSE [%] from 3.1% to 9.6%. Greatest reduction of RMSE [%] with PVEC was observed in wells of high radioactivity concentration, and decreased as a function of this activity. Without PVEC, well walls and surrounding areas gave apparent signals of intensity close to that of the least activity wells, but declined towards zero for PVE-corrected data. For FWHM in the range of $\pm$1 SD, good recovery (4.6–4.8%) was achieved in the high activity regions, but over-correction was observed for FWHM exceeding +1 SD, and under-correction with FWHM of less than −1 SD (Table 2, Fig. 4B).

Animal data

VOI-mask validation

Mean SUV in WT animals was 0.42 ($\pm$0.08) for the frontal cortex, and 0.47 ($\pm$0.10) for the cerebellum. Uncorrected PET concentrations expressed as error [%] were underestimated by 15.0% in frontal cortex and 11.5% in cerebellum. PVE-corrected data showed distinct overcorrection in frontal cortical regions for all masks when extracerebral regions were not considered (mean error: +38.8%), whereas better recovery was achieved when extracerebral regions were included in the PVEC model (mean error: −4.2%). The smaller frontal cortical VOI resulted in higher correction relative to cerebellum. Consequently, $SUVR_{CTX/CBL}$ values appeared overcorrected, while similar results were observed when a subdivision of intracerebral regions was performed. Subdividing extracerebral regions did not affect $SUVR_{CTX/CBL}$, but further lowered the error [%] of cortical and cerebellar regions. Mean $SUVR_{CTX/CBL}$ by autoradiography was 0.94 $\pm$ 0.02, with an error [%] of −3.7% by PET without correction. PVEC with the large CTX VOI resulted in better agreement with autoradiography compared to usage of the small CTX VOI.

In the above analyses, a 10-region-mask containing two frontal cortical (CTX_{LARGE}), a cerebellar, a mixed cerebral and six extracerebral VOIs emerged to be most valid, showing error reductions of 9.5% and 7.1% for CTX and CBL at a mean $SUVR_{CTX/CBL}$ error [%] of −2.2% compared to gamma counter and autoradiography. However, to enable hippocampal analyses for TG mice, we find a 13-region-mask with segmentation of the mixed cerebral region into hippocampus, high and low unspecific regions also to be suitable. A detailed overview of error [%] in all CTX_{LARGE} masks investigated within the validation process is provided in Fig. 5.

Application to longitudinal [^{18}F]-florbetaben PET data

Impact on VOI-based PET data. PVEC processing using the 10-region mask for the entire group of WT plus TG mice ($N = 43$) resulted in a correction of +19.4 $\pm$ 9.1% in the CTX_{LARGE} VOI. Significantly higher corrections were obtained for TG groups aged 16 months (+21.5 $\pm$ 9.1%; $p < 0.05$) and 20 months (+34.2 $\pm$ 12.0%; $p < 0.001$) for CTX_{LARGE} when compared to their baseline at 13 months (+14.3 $\pm$ 6.6%), while pooled WT animals (+15.2 $\pm$ 5.5%) did not show significant changes in contrast to 13 month old TG animals. CBL and MIX were corrected by a mean of +5.0 $\pm$ 2.0% and +2.4 $\pm$ 0.7%, respectively, which was not significantly different in TG or WT groups. For extracerebral VOIs, HGL was corrected significantly higher in WT animals compared to 20 month old TG mice, whereas FRO received a significantly lower correction in this contrast. Corresponding values with inclusion of extracerebral VOIs and statistical comparisons (ANOVA) for all evaluated groups are detailed in Table 3.

With PVEC, the magnitude of $SUVR_{CTX/CBL}$ increased in TG mice by 12.2% ($p < 0.005$) at 16 months, and by 36.4% ($p < 0.05$) at 20 months of age, in contrast to +5.5% at 16 months ($p < 0.005$) and +15.5% at 20 months ($p < 0.05$) without PVEC, all relative to corresponding baseline data (Fig. 6A). Plotting of all PVE-corrected $SUVR_{CTX/CBL}$ data versus uncorrected data gave a non-linear relationship, fitting well to an exponential function, i.e. $y = 1.16 \times^{2.04}$ (Fig. 6B).

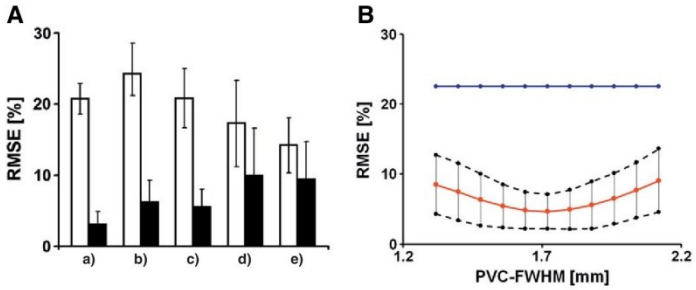

Fig. 4. (A) RMSE [%] $\pm$ SD for the five different radioactivity concentrations (a: 225.3; b: 182.7; c: 93.6; d: 61.3; e: 41.5 kBq/cc) as defined in Fig. 2A in uncorrected (white bars) and PVE-corrected (black bars; FWHM 1.72 mm) data. (B) PVE-correction with deviating FWHM parameters($\pm$5 SD) for the two high activities (a and b) indicates lower RMSE [%] (red line) with SDs (dashed lines) compared to uncorrected data (blue line) for the whole range, but best agreement at previously measured FWHM.

Table 2
Detailed RMSE [%] ± SD of PET results for five different cross-calibrated activities(a–e) in uncorrected and PVE-corrected (FWHM 1.72 mm ± 5 SDs) data.

Activity definition	Activimeter cross-calibrated activity (kBq/cc)	PET uncorrected (RMSE [%])	PET PVE-corrected FWHM 1.72 mm ± SDs (RMSE [%])										
			0 SD	+1 SD	+2 SD	+3 SD	+4 SD	+5 SD	−1 SD	−2 SD	−3 SD	−4 SD	−5 SD
a)	225.3	20.7 ± 2.2	3.1 ± 1.8	4.0 ± 2.5	5.4 ± 3.2	6.9 ± 3.3	8.5 ± 3.4	10.2 ± 3.5	2.7 ± 1.6	3.1 ± 1.7	3.9 ± 2.3	5.1 ± 2.7	6.2 ± 2.6
b)	182.7	24.3 ± 4.3	6.2 ± 3.1	5.9 ± 3.2	5.8 ± 3.8	6.1 ± 4.0	6.8 ± 4.1	7.9 ± 4.8	7.0 ± 3.6	7.9 ± 4.5	8.7 ± 5.2	9.8 ± 5.4	10.8 ± 5.3
c)	93.6	20.8 ± 4.2	5.6 ± 2.5	6.0 ± 3.0	6.8 ± 4.0	7.9 ± 4.9	9.2 ± 5.7	10.6 ± 6.4	5.4 ± 2.8	5.7 ± 3.7	6.2 ± 4.4	7.1 ± 4.3	7.9 ± 4.4
d)	61.3	17.3 ± 6.1	10.0 ± 6.6	11.3 ± 6.6	13.0 ± 6.6	14.7 ± 6.6	16.6 ± 6.7	18.5 ± 6.7	8.6 ± 6.6	7.5 ± 6.2	6.8 ± 5.7	6.3 ± 5.1	6.2 ± 4.2
e)	41.5	14.2 ± 3.9	9.5 ± 5.2	10.9 ± 5.4	12.5 ± 5.6	12.2 ± 5.8	16.0 ± 6.0	17.8 ± 6.2	7.9 ± 4.6	6.7 ± 4.1	5.6 ± 3.8	4.7 ± 3.1	4.2 ± 2.7

The $SUVR_{HIP/CBL}$ ratio did not show any significant changes when assessed by the 13-region-mask upon PVE-correction. Histological examination of this material showed amyloid plaques in only one TG animal at 20 months of age in hippocampus, in which individual PVEC increased the SUVR by 54.6%, versus a mean of only 18.4% in the histologically normal hippocampi of the four other aged TG mice.

Impact on correlation with histological and autoradiography data. Correlation of PET findings with histological results ex vivo was high ($R = 0.95$) for uncorrected and PVE-corrected data, with a greater slope in the latter case (Fig. 7A). $SUVR_{CTX/CBL}$ of PVE-corrected images agreed with autoradiographic results with a mean error [%] of 4.8 ± 1.5%, whereas there was lesser agreement for uncorrected $SUVR_{CTX/CBL}$ (18.9 ± 9.8%) (Fig. 7B). The two aged TG mice with especially abundant β-amyloid accumulation showed discrepancies of −25.2% and −29.3% in uncorrected $SUVR_{CTX/CBL}$, which declined to only −4.7% and −6.8% upon PVEC of the PET data.

Impact of PVEC on power calculations

PVEC increased the statistical power of all presumed therapy effect sizes, such that the detectability of significant group differences increased by up to 8.8% (Fig. 8). In the plausible case of a 50% ET on plaque load, sample size calculations for a power of 0.8 indicated a requirement for N = 14 animals, which was reduced to N = 12 for PVE-corrected data.

Discussion

We first performed phantom studies to define with precision the point-spread function of our small animal PET recordings, and then undertook the first use of PVEC applied to mouse data with a ligand for β-amyloid, the novel tracer [^{18}F]-florbetaben, which we have previously reported to reveal progressive amyloid accumulation in the brain of our APP-Swe mouse model (Rominger et al., 2013). In such studies, quantitation of PET signal arising from small brain regions of mouse brain is certain to be affected by spill-in and spillover. In an early application of the present PVEC method, which involves calculation of the geometric transfer matrix for a set of tissue segments, we found that time – activity curves measured for the dopamine tracer FDOPA were substantially increased in the human basal ganglia (Rousset et al., 2000). The spatial resolution of the tomograph used for that study (12 mm) was of the same order as the scale of relevant structures in human brain, i.e. the caudate and putamen. We now encounter an analogous problem in using an instrument with 1.7 mm resolution to measure tracer uptake in mouse brain. Indeed, Monte Carlo simulation studies for the case of the dopamine $D_{2/3}$ receptor ligand [^{11}C]-raclopride in rat striatum

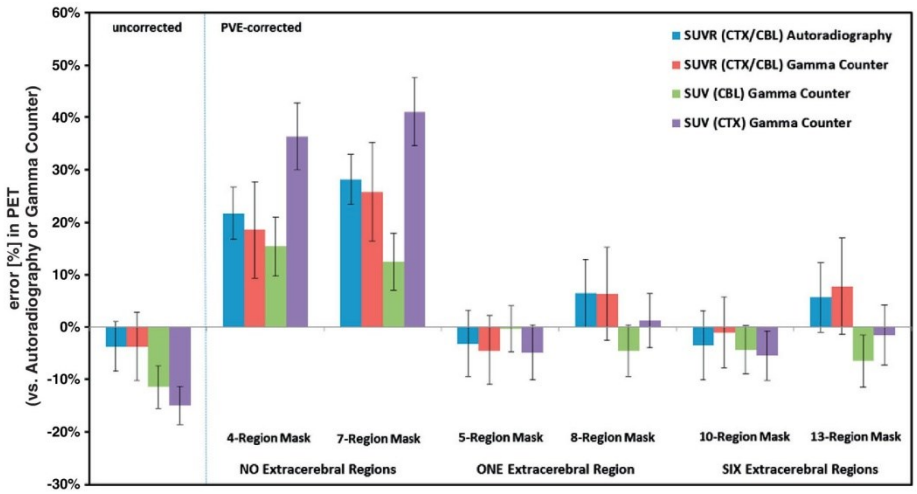

Fig. 5. Error [%] ± SD in PET SUVR and SUV for uncorrected and PVE-corrected data of six analyzed C57BL/6 animals when contrasted against autoradiography or gamma counter results. PVEC was performed with six different mask models, all containing the large frontal cortex VOI, either none, one or six extracerebral regions and four or seven intracerebral regions.

Table 3
Effects of correction [%] ± SD for single brain regions in combined animals (N = 43, column 2) and groups of APP-Swe and C57BL/6 animals (columns 3–6) after processing with the 10-region mask. Statistical differences are given as assessed by one-way ANOVA for each VOI (column 7). Significant group differences for APP-Swe (vs. APP-Swe baseline) and pooled WT animals (vs. any APP-Swe group) are marked with: *p < 0.05, **p < 0.001.

Region	Averaged groups 13–20 mo (correction [%])	APP-Swe 13 mo (correction [%])	APP-Swe 16 mo (correction [%])	APP-Swe 20 mo (correction [%])	C57BL/6 13–20 mo (correction [%])	One-way ANOVA
CTX-large	+19.4 ± 9.1	+14.3 ± 6.6	+21.5 ± 9.1*	+34.2 ± 12.1**	+15.2 ± 5.5	F = 9.13; p < 0.001
CBL	+4.8 ± 2.6	+5.0 ± 2.0	+5.1 ± 2.5	+4.9 ± 1.5	+4.6 ± 3.1	F = 0.07; p = n.s.
MIX	+1.7 ± 1.0	+1.5 ± 0.8	+1.6 ± 0.7	+1.3 ± 0.6	+1.9 ± 1.2	F = 2.22; p = n.s.
HGL	+38.3 ± 2.9	+37.5 ± 2.4	+35.7 ± 2.7	+35.0 ± 1.1	+40.1 ± 1.8**	F = 15.28; p < 0.001
FRO	−2.6 ± 2.9	−2.2 ± 2.0	−0.8 ± 2.5	−0.1 ± 1.8	−3.9 ± 2.8*	F = 5.06; p < 0.01
SPI	+30.2 ± 2.7	+31.2 ± 2.1	+31.6 ± 2.1	+30.3 ± 1.8	+29.4 ± 2.9	F = 1.96; p = n.s.
BAS	+12.3 ± 0.9	+12.6 ± 0.5	+12.6 ± 1.0	+11.2 ± 0.9	+12.4 ± 0.7	F = 2.11; p = n.s.
SUP	+27.6 ± 2.5	+27.8 ± 2.3	+26.5 ± 1.4	+29.1 ± 1.6	+27.5 ± 2.9	F = 1.15; p = n.s.
BGR	−58.7 ± 10.9	−58.3 ± 6.7	−57.6 ± 4.4	−61.5 ± 6.6	−58.6 ± 14.2	F = 0.13; p = n.s.

showed the occurrence of considerable bias, and improved fits upon application of the PVEC (Lehnert et al., 2012), and simulations likewise show considerable bias arising in quantitation of [^{18}F]-FDG tracer uptake in rat spinal cord (Nandoe Tewarie et al., 2010). Our present observations indicate improved precision and accuracy for the quantitation of β-amyloid in TG mouse brain, which will inform the rational design of future longitudinal studies testing potential disease-modifying treatments.

Phantom studies

Our uncorrected phantom measurements using sources emulating the size of relevant structures in mouse brain showed mean RMSE [%] of 19.5%, which is in concordance to results obtained for the simulation study of PVE for rat brain, cited above (Lehnert et al., 2012). We found that application of the VOI-based PVEC (Rousset et al., 1998) to the case of mouse brain reduced RMSE [%] to as low as 3.1%, notably in high activity sources designed to be comparable to small target regions in rodent PET studies. A prerequisite of this method is accurate knowledge of the FWHM of the tomograph in conjunction with optimal image reconstruction algorithms (Visser et al., 2009). We found for our instrument an isotropic FWHM of 1.72 mm, which gave the maximum reduction in RMSE [%] error, whereas significant miscorrection was observed when using FWHM deviating even slightly from the measured value (Fig. 4B).

PVEC algorithms

PVEC of human brain data has frequently been performed using the Müller-Gärtner method (Muller-Gartner et al., 1992), and its modifications (Erlandsson et al., 2012). This approach entails MR-based segmentation of gray and white matter, and voxelwise correction of gray matter, assuming uniform uptake throughout white matter. The Müller-Gärtner method is provided as an option in the commercial software PMOD, but is not readily applicable for small animal PET data. In our hands, segmentation of individual mouse MR images underestimates the white matter volumes in cerebellum and elsewhere, relative to large voxel sizes in PET, which propagates to inadequate Müller-Gärtner correction of PET data. This phenomenon is also present, however less apparent, in application to human PET data (Thomas et al., 2011).

The present VOI-based approach employs predefined masks in a brain template used for co-registration of individual PET images; the particular VOIs need only be tailored for the pattern of tracer uptake particular to the tracer in question. PET recordings of rodent brain are vulnerable to spill-in from extracerebral structures such as (for some tracers) the cranium (Mille et al., 2012; Rominger et al., 2010) and more frequently, the Harderian glands, which can substantially distort recordings in adjacent frontal brain structures (Fukuyama et al., 1998). In such cases, the segmented extracerebral sources can be included in the VOI-based PVEC, as in the present study.

Reconstruction parameters used at our small animal PET facility offer a nearly space-invariant spatial resolution (Qi and Leahy, 2000; Visser

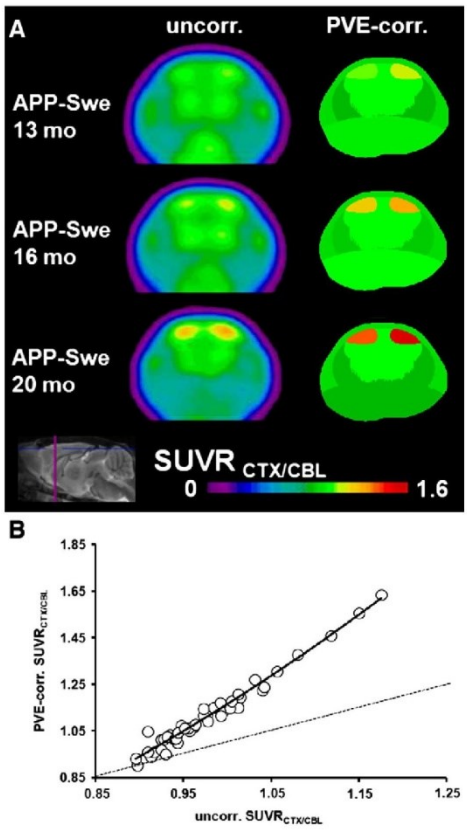

Fig. 6. (A) Coronal planes of mean [^{18}F]-florbetaben $SUVR_{CTX/CBL}$ uptake maps through ventral frontal cortex in APP-Swe mice of different ages, i.e. (baseline) 13, 16, and 20 months compared for uncorrected and PVE-corrected data. (B) $SUVR_{CTX/CBL}$ values plotted as a function of PVE-correction. Dotted line represents a linear zero correction.

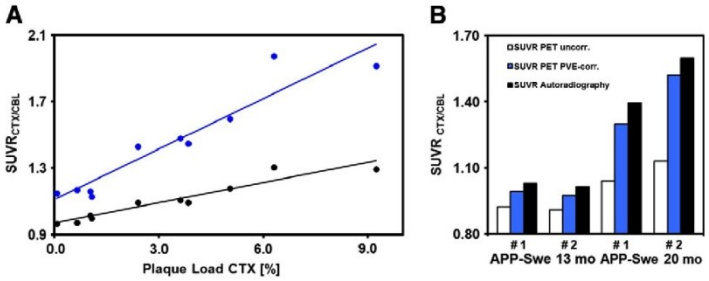

Fig. 7. (A) Correlation of percentage plaque load as determined from histochemistry (conducted in 10 hemispheres) with $SUVR_{CTX/CBL}$ analyses of [^{18}F]-florbetaben PET in group of APP-Swe mice aged 13–20 months for uncorrected (black dots and line) and PVE-corrected (blue dots and line) data. (B) Comparison of $SUVR_{CTX/CBL}$ in PET data (white bars = uncorrected; blue bars = PVE-corrected) with corresponding $SUVR_{CTX/CBL}$ in autoradiography (black bars) of two 13 months and two 20 months old APP-Swe mice.

et al., 2009). Phantom studies with cannulae and well-plates likewise reached the edges of the FoV and did not indicate any relevant deviation from this assumption. However, when reconstruction algorithms with a more variant spatial resolution are used, potential changes in FWHM have to be considered when moving away from the center of field (Mannheim et al., 2012). In such a circumstance we suggest making an assessment through line or point sources within the target space, since the magnitude of FWHM strongly influences VOI-based PVEC.

Mask validation

A simulation study of PVEC in rat brain found the inhomogeneous pattern of extracerebral uptake to be unsuited for definition of VOIs (Lehnert et al., 2012). However, when comparing PVEC-processed results with gold standard measurements of radioactivity concentrations, we observed an overcorrection of up to 32.3% when excluding extracerebral regions from consideration, whereas defining a single VOI encompassing extracerebral structures led to greater accuracy of brain corrections, despite the indisputably heterogeneous uptake in that VOI; subdividing the single extracerebral VOI into six regions further improved accuracy of the brain PVEC (Fig. 5).

Our approach to subdivision of basal cortical regions with inhomogeneous tracer uptake in WT and TG mice slightly lowered total radioactivity concentrations measured for CBL (−4.0%) and raised those for CTX(+3.9%). The location of the MIX-HI region in the vicinity of CBL and the MIX-LO region surrounding the periphery of the CTX VOI seems in this regard consistent with the functional principle of the VOI-based PVEC method, as all changes were in the expected direction. Nevertheless, inclusion of this subdivision resulted in 5.7% overestimation of $SUVR_{CTX/CBL}$ relative to autoradiography and gamma counter results. We suppose that this bias arose from instability of the PVEC with increasing number of VOIs within a small brain volume, as recognized in the original reports of the method (Rousset et al., 1998). Thus, optimal VOI-based PVEC must address the real heterogeneity of tissue uptake, without applying more tissue subdivisions than the PVEC method can support, in a typical trade-off between accuracy and precision.

Implementing cortical target VOIs (CTX) of small diameter in the scale of 1 mm resulted in a non-significant shift of $SUVR_{CTX/CBL}$ towards higher values (+2.1%) when compared with autoradiography. In general, our findings support the use of VOI-diameters scaled at least double the voxel dimension (1.6 mm in our case). In particular, our CTX_{LARGE} target VOI meets this requirement and gave stable $SUVR_{CTX/CBL}$ values after PVEC, which were accurate relative to gold standard measurements.

Application of PVEC to longitudinal [^{18}F]-florbetaben PET data

Our PET images of β-amyloid tracer accumulation in mouse brain appeared to be affected by PVE in two inter-related respects: First, pathology-free WT animals showed PVE-corrections of 12.3 ± 4.1% in cortical regions and 6.2 ± 2.1% in cerebellum, propagating to a very slight increase in binding ratios, concurring with the high agreement between corrected and uncorrected binding ratios in a study of mouse brain glucose metabolism (Toyama et al., 2004). As expected, our findings in the longitudinal study match those in the original WT group from the mask validation process, and can be readily attributed to the small size of the mouse brain (12 × 10 × 7 mm) relative to the tomograph resolution (isotropic 1.7 mm); the entire mouse brain thus contains only some 150 resolution elements, a circumstance comparable to analyzing human brain images at a resolution of 20 mm. Second, we found that PVEC increased the cortical signal in TG mice by up to 53.4%, as a function of increasing plaque load, which was verified relative to gold standard findings post mortem. In practice, histological examination reveals our [^{18}F]-florbetaben ß-amyloid imaging in TG mice to be derived from signal from hotspots measuring only 9–15 mm^3 in volume, which are embedded in a cool surround, with tracer uptake similar to that in the reference region. Thus, the target-to-background ratio without PVEC is unity in WT and young TG mice, but increases to

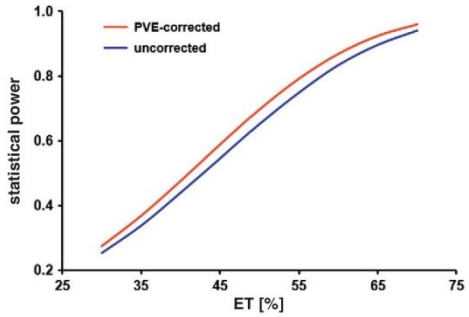

Fig. 8. Power calculation for Δ-$SUVR_{CTX/CBL}$-[%] comparisons by extrapolation of possible treatment effects (ET [%]). Based on paired *t*-tests of longitudinal APP-Swe mice (N = 8; 13 and 16 months) statistical power is depicted for uncorrected (blue line) and PVE-corrected (red line) data.

approximately 1.6 in aged TG mice with heavy plaque load (Rominger et al., 2013). An earlier phantom study investigating PVE arising with the Inveon DPET (Mannheim et al., 2012) likewise revealed that PVE increased with higher uncorrected target-to-background ratios, just as we see in our summary plot of PVE-corrected versus uncorrected [^{18}F]-florbetaben ratios in aging TG mice (Fig. 6B).

The correlation of PET results in vivo with autoradiographic data ex vivo in TG mice further highlights the benefits of PVEC in longitudinal studies, in that discrepancies between PET and autoradiographic $SUVR_{CTX/CBL}$ measurements noted previously (Rominger et al., 2013) were dramatically reduced, indicating improved accuracy of PET, without penalty in precision. Our findings of differing PET and autoradiography SUVR in the previous [^{18}F]-florbetaben study matches earlier findings with [^{18}F]-florbetapir, a similar ß-amyloid tracer (Poisnel et al., 2012) and emphasizes the necessity of PVE-correction in small animal ß-amyloid studies. This favorable state of affairs may be in part related to our use of a simple uptake ratio as our endpoint; in the earlier human FDOPA PET study, PVEC resulted in greater accuracy of kinetic estimates, but with loss of precision, which was most pronounced in analyses employing a complex, multi-parameter FDOPA kinetic model (Rousset et al., 2000).

The overall correlation of PET data to histological and autoradiographic results depicted in Fig. 7A was equally high ($R = 0.95$) with and without PVEC, but with a greater slope after correction, which is another indication of improved accuracy without loss of precision.

In one previous PET study of ß-amyloid with [^{18}F]-FDDNP in Tg2576 mice, $SUVR_{CTX/CBL}$ was paradoxically lower compared to WT animals, which the authors attributed to a consequence of PVE and limited spatial resolution of their scanner (Kuntner et al., 2009). However, we do not expect that a VOI-based PVEC approach could invert such results, unless the PET images were confounded by extensive extracerebral spill-in in one group, but not the other. Since we saw similar patterns of tracer uptake in TG and WT animals apart from the β-amyloid accumulating regions, we can exclude this un-parsimonious explanation.

Conclusion

Application of VOI-based PVEC in [^{18}F]-florbetaben PET studies of β-amyloid accumulation in aging APP-Swe mice improves quantitation of the PET signal, and power analysis predicts that fewer animals per group will be required to detect treatment effects in future longitudinal studies. The small reduction in group size may not be decisive in the planning of experiments, but the benefit of improved accuracy of PET measurements relative to gold standard findings is in itself compelling grounds for undertaking the PVEC.

Supplementary data to this article can be found online at http://dx.doi.org/10.1016/j.neuroimage.2013.09.017.

Acknowledgments

We thank Rosel Oos, Karin Bormann-Giglmaier and Matthias Moser for the excellent technical support.

References

Cheng, J.C., Shoghi, K., Laforest, R., 2012. Quantitative accuracy of MAP reconstruction for dynamic PET imaging in small animals. Med. Phys. 39, 1029–1041.

Erlandsson, K., Buvat, I., Pretorius, P.H., Thomas, B.A., Hutton, B.F., 2012. A review of partial volume correction techniques for emission tomography and their applications in neurology, cardiology and oncology. Phys. Med. Biol. 57, R119–R159.

Fukuyama, H., Hayashi, T., Katsumi, Y., Tsukada, H., Shibasaki, H., 1998. Issues in measuring glucose metabolism of rat brain using PET: the effect of harderian glands on the frontal lobe. Neurosci. Lett. 255, 99–102.

Klunk, W.E., Bacskai, B.J., Mathis, C.A., Kajdasz, S.T., McLellan, M.E., Frosch, M.P., Debnath, M.L., Holt, D.P., Wang, Y., Hyman, B.T., 2002. Imaging Abeta plaques in living transgenic mice with multiphoton microscopy and methoxy-X04, a systemically administered Congo red derivative. J. Neuropathol. Exp. Neurol. 61, 797–805.

Klunk, W.E., Lopresti, B.J., Ikonomovic, M.D., Lefterov, I.M., Koldamova, R.P., Abrahamson, E.E., Debnath, M.L., Holt, D.P., Huang, G.F., Shao, L., DeKosky, S.T., Price, J.C., Mathis, C.A., 2005. Binding of the positron emission tomography tracer Pittsburgh compound-B reflects the amount of amyloid-beta in Alzheimer's disease brain but not in transgenic mouse brain. J. Neurosci. 25, 10598–10606.

Kuntner, C., Kesner, A.L., Bauer, M., Kremslehner, R., Wanek, T., Mandler, M., Karch, R., Stanek, J., Wolf, T., Muller, M., Langer, O., 2009. Limitations of small animal PET imaging with [^{18}F]FDDNP and FDG for quantitative studies in a transgenic mouse model of Alzheimer's disease. Mol. Imaging Biol. 11, 236–240.

Lehnert, W., Gregoire, M.C., Reilhac, A., Meikle, S.R., 2012. Characterisation of partial volume effect and region-based correction in small animal positron emission tomography (PET) of the rat brain. NeuroImage 60, 2144–2157.

Maeda, J., Ji, B., Irie, T., Tomiyama, T., Maruyama, M., Okauchi, T., Staufenbiel, M., Iwata, N., Ono, M., Saido, T.C., Suzuki, K., Mori, H., Higuchi, M., Suhara, T., 2007. Longitudinal, quantitative assessment of amyloid, neuroinflammation, and anti-amyloid treatment in a living mouse model of Alzheimer's disease enabled by positron emission tomography. J. Neurosci. 27, 10957–10968.

Mannheim, J.G., Judenhofer, M.S., Schmid, A., Tillmanns, J., Stiller, D., Sossi, V., Pichler, B.J., 2012. Quantification accuracy and partial volume effect in dependence of the attenuation correction of a state-of-the-art small animal PET scanner. Phys. Med. Biol. 57, 3981–3993.

Manook, A., Yousefi, B.H., Willuweit, A., Platzer, S., Reder, S., Voss, A., Huisman, M., Settles, M., Neff, F., Velden, J., Schoor, M., von der Kammer, H., Wester, H.J., Schwaiger, M., Henriksen, G., Drzezga, A., 2012. Small-animal PET imaging of amyloid-beta plaques with [^{11}C]PiB and its multi-modal validation in an APP/PS1 mouse model of Alzheimer's disease. PLoS One 7, e31310.

Mille, E., Cumming, P., Rominger, A., La Fougere, C., Tatsch, K., Wangler, B., Bartenstein, P., Boning, G., 2012. Compensation for cranial spill-in into the cerebellum improves quantitation of striatal dopamine D(2)/(3) receptors in rats with prolonged [(1)(8)F]-DMFP infusions. Synapse 66, 705–713.

Muller-Gartner, H.W., Links, J.M., Prince, J.L., Bryan, R.N., McVeigh, E., Leal, J.P., Davatzikos, C., Frost, J.J., 1992. Measurement of radiotracer concentration in brain gray matter using positron emission tomography: MRI-based correction for partial volume effects. J. Cereb. Blood Flow Metab. 12, 571–583.

Nandoe Tewarie, R.D., Yu, J., Seidel, J., Rahiem, S.T., Hurtado, A., Tsui, B.M., Grotenhuis, J.A., Pomper, M.G., Oudega, M., 2010. Positron emission tomography for serial imaging of the contused adult rat spinal cord. Mol. Imaging 9, 108–116.

Poisnel, G., Dhilly, M., Moustie, O., Delamare, J., Abbas, A., Guilloteau, D., Barre, L., 2012. PET imaging with [^{18}F]AV-45 in an APP/PS1-21 murine model of amyloid plaque deposition. Neurobiol. Aging 33, 2561–2571.

Qi, J., Leahy, R.M., 2000. Resolution and noise properties of MAP reconstruction for fully 3-D PET. IEEE Trans. Med. Imaging 19, 493–506.

Richards, J.G., Higgins, G.A., Ouagazzal, A.M., Ozmen, L., Kew, J.N., Bohrmann, B., Malherbe, P., Brockhaus, M., Loetscher, H., Czech, C., Huber, G., Bluethmann, H., Jacobsen, H., Kemp, J.A., 2003. PS2APP transgenic mice, coexpressing hPS2mut and hAPPswe, show age-related cognitive deficits associated with discrete brain amyloid deposition and inflammation. J. Neurosci. 23, 8989–9003.

Rojas, S., Herance, J.R., Gispert, J.D., Abad, S., Torrent, E., Jimenez, X., Pareto, D., Perpina, U., Sarroca, S., Rodriguez, E., Ortega-Aznar, A., Sanfeliu, C., 2013. In vivo evaluation of amyloid deposition and brain glucose metabolism of 5XFAD mice using positron emission tomography. Neurobiol. Aging 34, 1790–1798.

Rominger, A., Wagner, E., Mille, E., Boning, G., Esmaeilzadeh, M., Wangler, B., Gildehaus, F.J., Nowak, S., Bruche, A., Tatsch, K., Bartenstein, P., Cumming, P., 2010. Endogenous competition against binding of [(^{18})F]DMFP and [(^{18})F]fallypride to dopamine D(2/3) receptors in brain of living mouse. Synapse 64, 313–322.

Rominger, A., Brendel, M., Burgold, S., Keppler, K., Baumann, K., Xiong, G., Mille, E., Gildehaus, F.J., Carlsen, J., Schlichtiger, J., Niedermoser, S., Wangler, B., Cumming, P., Steiner, H., Herms, J., Haass, C., Bartenstein, P., 2013. Longitudinal assessment of cerebral beta-amyloid deposition in mice overexpressing Swedish mutant beta-amyloid precursor protein using ^{18}F-florbetaben PET. J. Nucl. Med. 54, 1127–1134.

Rousset, O.G., Ma, Y., Evans, A.C., 1998. Correction for partial volume effects in PET: principle and validation. J. Nucl. Med. 39, 904–911.

Rousset, O.G., Deep, P., Kuwabara, H., Evans, A.C., Gjedde, A.H., Cumming, P., 2000. Effect of partial volume correction on estimates of the influx and cerebral metabolism of 6-[(^{18})F]fluoro-L-dopa studied with PET in normal control and Parkinson's disease subjects. Synapse 37, 81–89.

Rousset, O.G., Collins, D.L., Rahmim, A., Wong, D.F., 2008. Design and implementation of an automated partial volume correction in PET: application to dopamine receptor quantification in the normal human striatum. J. Nucl. Med. 49, 1097–1106.

Singh, S., Kushwah, A.S., Singh, R., Farswan, M., Kaur, R., 2012. Current therapeutic strategy in Alzheimer's disease. Eur. Rev. Med. Pharmacol. Sci. 16, 1651–1664.

Snellman, A., Rokka, J., Lopez-Picon, F.R., Eskola, O., Wilson, I., Farrar, G., Scheinin, M., Solin, O., Rinne, J.O., Haaparanta-Solin, M., 2012. Pharmacokinetics of [^{18}F]flutemetamol in wild-type rodents and its binding to beta amyloid deposits in a mouse model of Alzheimer's disease. Eur. J. Nucl. Med. Mol. Imaging 39, 1784–1795.

Teipel, S.J., Buchert, R., Thome, J., Hampel, H., Pahnke, J., 2011. Development of Alzheimer-disease neuroimaging-biomarkers using mouse models with amyloid-precursor protein-transgene expression. Prog. Neurobiol. 95, 547–556.

Thomas, B.A., Erlandsson, K., Modat, M., Thurfjell, L., Vandenberghe, R., Ourselin, S., Hutton, B.F., 2011. The importance of appropriate partial volume correction for

PET quantification in Alzheimer's disease. Eur. J. Nucl. Med. Mol. Imaging 38, 1104–1119.
Toyama, H., Ichise, M., Liow, J.S., Vines, D.C., Seneca, N.M., Modell, K.J., Seidel, J., Green, M.V., Innis, R.B., 2004. Evaluation of anesthesia effects on [18F]FDG uptake in mouse brain and heart using small animal PET. Nucl. Med. Biol. 31, 251–256.
Toyama, H., Ye, D., Ichise, M., Liow, J.S., Cai, L., Jacobowitz, D., Musachio, J.L., Hong, J., Crescenzo, M., Tipre, D., Lu, J.Q., Zoghbi, S., Vines, D.C., Seidel, J., Katada, K., Green, M.V., Pike, V.W., Cohen, R.M., Innis, R.B., 2005. PET imaging of brain with the beta-amyloid probe, [11C]6-OH-BTA-1, in a transgenic mouse model of Alzheimer's disease. Eur. J. Nucl. Med. Mol. Imaging 32, 593–600.
Videen, T.O., Perlmutter, J.S., Mintun, M.A., Raichle, M.E., 1988. Regional correction of positron emission tomography data for the effects of cerebral atrophy. J. Cereb. Blood Flow Metab. 8, 662–670.
Villemagne, V.L., Ong, K., Mulligan, R.S., Holl, G., Pejoska, S., Jones, G., O'Keefe, G., Ackerman, U., Tochon-Danguy, H., Chan, J.G., Reininger, C.B., Fels, L., Putz, B., Rohde, B., Masters, C.L., Rowe, C.C., 2011. Amyloid imaging with(18)F-florbetaben in Alzheimer disease and other dementias. J. Nucl. Med. 52, 1210–1217.
Virdee, K., Cumming, P., Caprioli, D., Jupp, B., Rominger, A., Aigbirhio, F.I., Fryer, T.D., Riss, P.J., Dalley, J.W., 2012. Applications of positron emission tomography in animal models of neurological and neuropsychiatric disorders. Neurosci. Biobehav. Rev. 36, 1188–1216.
Visser, E.P., Disselhorst, J.A., Brom, M., Laverman, P., Gotthardt, M., Oyen, W.J., Boerman, O.C., 2009. Spatial resolution and sensitivity of the Inveon small-animal PET scanner. J. Nucl. Med. 50, 139–147.
Ziegler-Graham, K., Brookmeyer, R., Johnson, E., Arrighi, H.M., 2008. Worldwide variation in the doubling time of Alzheimer's disease incidence rates. Alzheimers Dement. 4, 316–323.

Eidesstattliche Versicherung

_____
Name, Vorname

Ich erkläre hiermit an Eides statt,

dass ich die vorliegende Dissertation mit dem Thema:

Untersuchungen der Amyloid-Pathologie an einem transgenen Alzheimer-Mausmodell mittels Positronen-Emissions-Tomographie

selbständig verfasst, mich außer der angegebenen keiner weiteren Hilfsmittel bedient und alle Erkenntnisse, die aus dem Schrifttum ganz oder annähernd übernommen sind, als solche kenntlich gemacht und nach ihrer Herkunft unter Bezeichnung der Fundstelle einzeln nachgewiesen habe. Ich erkläre des Weiteren, dass die hier vorgelegte Dissertation nicht in gleicher oder in ähnlicher Form bei einer anderen Stelle zur Erlangung eines akademischen Grades eingereicht wurde.

_____ _____
Ort, Datum Unterschrift Doktorandin/Doktorand